Variability in drift ice export from the Arctic Ocean to the North Icelandic Shelf over the last 8,000 years: a multi-proxy evaluation

Patricia Cabedo-Sanz [a], Simon T. Belt[a]*, Anne E Jennings[b,c], John T. Andrews[b,c] and Áslaug Geirsdóttir [d]

(a) Biogeochemistry Research Centre, School of Geography, Earth and Environmental Sciences, Plymouth University, Drake Circus, Plymouth, PL4 8AA, UK

(b) INSTAAR, University of Colorado, Boulder, CO 80309, USA

(c) Department of Geological Sciences, University of Colorado, Boulder, CO, 80309, USA

(d) Department of Earth Sciences, University of Iceland, IS-101, Reykjavík, Iceland

* Author for correspondence

Professor Simon T Belt
Biogeochemistry Research Centre
Plymouth University
Drake Circus, Plymouth
PL4 8AA
UK

e-mail: sbelt@plymouth.ac.uk
Phone: +44 (0)1752 584959
FAX: +44 (0)1752 584709

1

1 **Abstract**

2

3 North Iceland represents a climatically sensitive region, in part, due to its location at the

4 confluence of southward flowing and drift ice-laden polar waters from the Arctic Ocean

5 delivered by the East Greenland Current, and the relatively warm and saline Irminger

6 Current, a northerly flowing branch of the North Atlantic Current. Despite its pivotal

7 location, there is a paucity of high resolution and long-term sea ice records for the region,

8 with some disparities in certain previous investigations. Here, the identification of the

9 biomarker IP_{25} as a reliable proxy for drift ice for North Iceland has been confirmed by

10 measuring its abundance in surface sediments from the region and comparison of outcomes

11 with documentary records of sea ice and other proxy data. By analysing IP_{25} in a well-dated

12 marine sediment core from the North Icelandic Shelf (NIS) (MD99-2269), we also provide a

13 high resolution (ca. 25 yr) record of drift sea ice for the region and complement this with a

14 lower resolution record (ca. 100 yr) obtained from a second core site, located further east

15 (JR51-GC35). Statistical treatment of equi-spaced time series reveals strong linear

16 correlations between IP_{25} and a further drift ice proxy (quartz) in each core. Thus, linear

17 regression analysis between both proxies gave correlation coefficients (R^2) of 0.74 and 0.66

18 for MD99-2269 (25 yr) and JR51-GC35 (100 yr), respectively. Further, the individual proxies

19 were well correlated between the two cores, with R=0.91 and 0.77 for IP_{25} and quartz,

20 respectively. The IP_{25}-based sea ice record for MD99-2269, combined with other new

21 biomarker and foraminifera data, and previously published proxy data for primary

22 productivity and sea surface temperature, suggest that the paleoceanographic evolution for

23 the NIS over the last 8 ka can be classified into three main intervals. The early mid Holocene

24 (ca 8–6.2 cal ka BP) was characterized by relatively low or absent drift ice, low primary

25 productivity and relatively high SSTs. During the mid-Holocene (ca 6.2–3.3 cal ka BP), drift

26 ice increased concomitant with decreasing SSTs, although primary productivity was

27   somewhat enhanced during this interval. IP_{25} first reached its mean value for the entire record

28   at ca 5 cal ka BP, before increasing, continuously, ca 4.3 cal ka BP, broadly in line with the

29   onset of Neoglaciation as seen in some other proxy records. Further increases in drift ice were

30   evident during the late Holocene (ca 3.3 cal ka BP to present), culminating in maximum sea

31   ice during the Little Ice Age. In addition, the IP_{25} record from MD99-2269 shows some

32   positive regime shifts from the general trend, especially at ca 3.8, 2.7, 1.5, 0.7 and 0.4 cal ka

33   BP, that have analogs in some other paleoceanographic reconstructions influenced by the

34   East Greenland Current. The abrupt increases in IP_{25} at ca 1.5 and 0.7 cal ka BP are

35   coincident with rapid cooling identified previously in an Icelandic lacustrine temperature

36   record, suggesting significant coupling between the marine and terrestrial systems. The

37   contribution of sea ice to the broader climate system is further evidenced through the

38   identification of statistically significant periodicities (ca 1000 yr and ca 200–230 yr) in the

39   drift ice proxy data that have counterparts in previous studies concerning atmospheric and

40   oceanic variability and solar forcing mechanisms.

41   **1 – Introduction**

42   Sea ice plays a key role in determining the energy balance at high latitudes by influencing the

43   exchange of heat, gases and moisture between the polar oceans and the atmosphere. By

44   reflecting much of the incoming solar radiation, sea ice also insulates the cold polar

45   atmosphere from the relatively warm ocean in winter. Changes in Arctic Ocean sea ice

46   dimensions have received considerable attention in recent years, largely because of its recent

47   and dramatic decline (e.g., Goosse et al., 2013; Schiermeier, 2012; Serreze et al., 2007).

48   However, due to its strong positive feedback mechanism in controlling global climate, the

49   role of sea ice through the geological record is also of considerable interest. For example,

50   expanded sea ice has been suggested to play an important role in maintaining the unusual

51   duration of mostly cold summers during the little ice age (LIA) (Lehner et al., 2013; Miller et

52   al., 2012; Schleussner and Feulner, 2013), and greatly reduced sea ice is necessary to explain

53   the warmth of the mid-Pliocene (Haywood and Valdes, 2004). However, since only a very

54   few observational records of past sea ice exist (e.g. Bergthorsson, 1969; de la Mare, 1997;

55   Divine and Dick, 2006; Ogilvie and Jónsdóttir, 2000), paleo sea ice reconstructions rely

56   heavily on proxy-based methods, so the development and application of sea ice proxies have

57   also received considerable attention in recent years (de Vernal et al., 2013a; Polyak et al.,

58   2010). Some sea ice proxies have a biological origin and are typically based on species

59   assemblages of diatoms, dinoflagellate cysts (dinocysts), ostracods and foraminifera (e.g.,

60   Justwan and Koç, 2008; Cronin et al., 2013; de Vernal et al., 2013b,c; Seidenkrantz, 2013) or

61   the occurrence and distribution of marine mammal remains and driftwood from raised

62   beaches (Dyke et al., 1996; Funder et al., 2011; Furze et al., 2014), while others rely on the

63   identification of material entrained within the ice itself (i.e. ice-rafted debris (IRD)) and

64   deposited in underlying marine sediments following ice melt (Andrews, 2009; Moros et al.,

65   2006). Despite the range of sea ice proxies, however, there is as yet, no strong consensus on

66   the changing dimensions of Arctic Ocean sea ice over the past 8 ka, although there is growing

67   evidence for a strong regional dependence (de Vernal et al., 2013c).

68

69   In recent years, the analysis of the biomarker IP_{25} (Belt et al., 2007), a C_{25} highly branched

70   isoprenoid (HBI) lipid made by certain Arctic sea ice diatoms (Brown et al., 2014), has been

71   suggested to provide a more direct measure of past sea ice when detected in underlying

72   sediments (a recent review is provided by Belt and Müller, 2013). Significantly, IP_{25} is stable

73   in sediments for millions of years (Knies et al., 2014) and has a stable isotopic composition

74   ($\delta^{13}C$) that is highly characteristic of a sea ice origin (Belt et al., 2008). Sedimentary IP_{25} is

75   generally interpreted as an indication of spring/early summer sea ice conditions due to its

76   formation by sea ice diatoms during the spring bloom (Brown et al., 2011; Belt et al., 2013).

77

78   To date, the main applications of IP_{25} for Holocene sea ice reconstruction have been carried

79   out for regions such as the Barents Sea (Belt et al., 2015; Berben et al., 2014; Vare et al.,

80   2010), the Canadian Arctic Archipelago (Belt et al., 2010; Vare et al., 2009), Fram Strait

81   (Müller et al., 2009, 2012) and the Laptev Sea (Fahl and Stein, 2012). On the other hand,

82   relatively little attention has been given to the East Greenland shelf and North Iceland,

83   although a low resolution study conducted for Foster Bugt on the central East Greenland shelf

84   indicated relatively stable sea ice conditions for most of the Holocene apart from the last ca

85   1.4 cal ka BP (Müller et al., 2012; Perner et al., 2015). This paucity of research is somewhat

86   surprising given that the East Greenland shelf is a very sensitive area to changes in sea ice

87   and freshwater outflow from the Arctic Ocean (e.g. Jennings and Weiner, 1996), while the

88   East Greenland Current (EGC), which flows adjacent to the East Greenland shelf, is one of

89   the main sea ice and freshwater export pathways from the Arctic Ocean (Aagaard and

90   Coachman, 1968) towards the Denmark Strait region (i.e. South-East Greenland and North

5

91   Iceland) as evidenced by the Great Salinity Anomaly of 1969 (Belkin et al., 1998; Dickson et

92   al., 1988). However, the first temporal IP_{25}-based sea ice reconstruction was carried out on a

93   core from the North Icelandic Shelf (NIS) (Massé et al., 2008) and showed that IP_{25}

94   concentrations were very well correlated with documented records of sea ice around Iceland

95   over the last ca. 1 ka (Ogilvie and Jónsson, 2001). The outcomes from this initial study by

96   Massé et al. (2008) were subsequently reinforced by analysis of three further cores from N,

97   NW and SW Iceland (Andrews et al., 2009a; Axford et al., 2011; Sicre et al., 2013).

98   Interestingly, the initial IP_{25} record from Massé et al. (2008) also closely matches the

99   reconstructed expansion of the Langjökull ice cap, Iceland (Larsen et al., 2011), and a

100 composite terrestrial record (Haukadalsvatn and Hvítárvatn, Iceland) (Geirsdóttir et al.,

101 2013), suggesting a close link between terrestrial Icelandic summer temperatures and changes

102 in sea ice cover in the adjacent ocean. However, each of these previous IP_{25}-based sea ice

103 reconstructions for the East Greenland shelf and North Iceland were either of low resolution,

104 temporally limited, or both. As such, there have been no high-resolution and long-term (e.g.

105 Holocene) IP_{25}-based sea ice reconstructions for this climatically sensitive region.

106

107 In the current study, we quantified IP_{25} in surface sediments and two marine cores (MD99-

108 2269 and JR51-GC35) from the NIS in order to both confirm the suitability of this biomarker

109 as a drift ice proxy and also to gain further insights into the spatial and temporal sea ice

110 evolution throughout the last 8 ka. In the first instance, therefore, we determined the

111 distribution of IP_{25} in surface sediments from the region and compared outcomes with known

112 modern sea ice conditions and a further drift ice proxy (i.e. quartz; Andrews, 2009). We then

113 investigated the IP_{25} content in the giant Calypso core MD99-2269, an exceptionally well-

114 dated high-resolution marine sediment record (Stoner et al., 2007) from ca 66° N on the NIS

115 (Fig. 1a) and situated at the boundary between major oceanic and atmospheric circulation

116   systems (Hopkins, 1991). In some recent IP_{25}-based Arctic sea ice reconstructions, combining

117   IP_{25} concentrations with those of certain phytoplankton biomarkers (typically sterols) in the

118   form of the so-called PIP_{25} index (Müller et al., 2011) has provided further insights into paleo

119   sea ice conditions, most notably from a semi-quantitative perspective (e.g., Müller et al.,

120   2011,2012,2014; Fahl and Stein, 2012; Xiao et al, 2015; Hörner et al., 2016; Smik et al.,

121   2016). However, since the conceptual model that underpins the PIP_{25} index (viz. a stable

122   winter ice margin with ice retreat during spring/summer) is not appropriate for the drift

123   conditions pertinent to the NIS, we refrained from measuring PIP_{25} indices within the current

124   study. We also note that, as yet, there has been no surface sediment-based calibration of the

125   PIP_{25} index for North Iceland, although it has been suggested previously that such an

126   approach may not be especially useful for regions of low sea ice cover (Navarro-Rodriguez et

127   al., 2013), as is the case for the NIS.

128

129   Several other climate proxy datasets are, however, available from MD99-2269 at various

130   resolutions that span the full 8 ka and beyond (e.g. Andersen et al., 2004b; de Vernal et al.,

131   2013b; Giraudeau et al., 2004; Justwan et al., 2008; Kristjánsdóttir et al., 2007; Moros et al.,

132   2006; Solignac et al., 2006) but it remains unclear which (if any) provide a secure record of

133   changes in sea ice, especially as some show divergence in outcomes (de Vernal et al., 2013b;

134   Moros et al., 2006; Solignac et al., 2006) and further conflicting evidence of Holocene

135   climate evolution exists between some of the other proxy datasets, especially after 3 ka BP.

136   For example, mineralogical-based sea ice (Moros et al., 2006) and microfossil-derived

137   bottom water temperature proxies indicate continued cooling after ca 3 cal ka BP (e.g.

138   Giraudeau et al., 2004; Kristjánsdóttir et al., 2007), while diatom transfer functions and

139   dinocyst distributions suggest late Holocene warming from around 2.5 ka BP (e.g. Justwan et

140   al., 2008; Solignac et al., 2006). Additionally, none of these records were investigated for

141 possible step-like responses or regime shifts of the type subsequently reconstructed from

142 terrestrial Iceland records (Geirsdóttir et al., 2013). To produce a more comprehensive

143 account of the changes in Holocene sea ice and surface water mass characteristics for the

144 region, we also compare our IP_{25} record from MD99-2269 with previous mineralogical

145 (quartz) data and new microfossil (planktic foraminifera) and other biomarker data, including

146 those for a tri-unsaturated highly branched isoprenoid (HBI) lipid (hereafter referred to as

147 $C_{25:3}$) produced by certain (as yet unidentified) diatoms, some of which are believed to thrive

148 in polar and sub-polar waters (Belt et al., 2008, 2015; Massé et al., 2011) and may, therefore,

149 provide further insights into phytoplankton productivity in such settings. In addition, we

150 compare our high resolution proxy records from MD99-2269 with further new IP_{25} and

151 previous quartz and alkenone SST records (albeit at lower resolution) obtained from a second

152 core (JR51-GC35) located further east, and with an integrated account of terrestrial Icelandic

153 climate, compiled previously (Andrews et al., 2014; Bendle and Rosell-Melé, 2007;

154 Geirsdóttir et al., 2013).

155

156 **2 – Regional setting**

157 The two main currents that characterise the Denmark Strait area are the East Greenland

158 Current (EGC) and the Irminger Current (IC) (Fig. 1a). The EGC is a cold, low-salinity polar

159 water current that flows southward along the Greenland margin, carrying sea ice and

160 freshwater from the Arctic Ocean (Aagaard and Coachman, 1968). Similarly, the EGC

161 branches out towards western and northern Iceland as the East Iceland Current (EIC)

162 (Malmberg, 1985). Freshwater and icebergs discharged from the Greenland Ice Sheet are

163 incorporated into the EGC as it flows southwards (Aagaard and Coachman, 1968; Rudels et

164 al., 2002). The IC is a branch of the North Atlantic Current (NAC) and flows northward,

165 carrying warm and saline Atlantic waters from the south (Fig. 1a). The IC splits close to

166 Denmark Strait; one branch flows northwards and clockwise along the West Iceland Shelf as

167 the North Iceland Irminger Current (NIIC), while the other is directed southwards and

168 counter-clockwise along south-east Greenland, entering the Kangerdlugssuaq Trough as an

169 intermediate layer between the polar water and the Atlantic intermediate water of the EGC

170 (e.g. Jennings et al., 2011).

171

172 The NIS is located at the boundary between major oceanic and atmospheric circulation

173 systems (Belkin et al., 2009). As such, it encapsulates the oceanographic and atmospheric

174 variability of a much broader region and represents a sensitive area for monitoring North

175 Atlantic climate (Hopkins, 1991), which has made it a target for several previous

176 paleoceanographic studies (e.g. Andersen et al., 2004b; Giraudeau et al., 2004; Knudsen et

177 al., 2004; Solignac et al., 2006).

178

179 The location of the main core here (MD99-2269) sits between two of the routinely surveyed

180 hydrographic sections on the NIS, Siglunes and Hornbanki (Fig. 1b). MD99-2269 lies close

181 to the North Iceland Marine Front, which separates warm Atlantic waters from cold

182 polar/Arctic water (Belkin et al., 2009). The Arctic water of the EIC is usually too saline to

183 form sea ice *in situ*, although during times of strong advection of low salinity polar water

184 from the EGC, the EIC surface water both forms and transports sea ice (e.g. Ólafsson, 1999).

185 The historical seasonal limit of Arctic drift ice, carried southward by the EGC, lies close to

186 Iceland (Ogilvie, 1996), making the region extremely suitable area for investigating changes

187 to drift ice conditions in the past (Bergthorsson, 1969; Koch, 1945). MD99-2269 is located

188 <100 km south of the average April AD 1870–1920 sea ice edge position in the northern

189 North Atlantic (Fig. 2a, Divine and Dick, 2006).

190

191 **3 – Material and methods**

9

192   *3.1 Field methods and chronology*

193   Surface sediment samples were collected from 30 sites across west and north Iceland during

194   the *Bjarni Saemundsson* B997 cruise in 1997 (Fig. 1 and Supplementary Table 1, Helgadóttir,

195   1997).

196

197   Core MD99-2269 was recovered in Húnaflói on the NIS (66$^\mathbf{o}$37.53 N, 20$^\mathbf{o}$51.16 W, water

198   depth 365 m, core length 2533 cm; Fig 1a) on board the R/V *Marion Dufresne II* during the

199   summer of 1999 as part of the international IMAGES-V (International Marine Past Global

200   Change Study) campaign. The age model for MD99-2269 was developed by Stoner et al.

201   (2007) and is based on 27 accelerator mass spectrometry (AMS) ^{14}C dates, tephrochronology

202   and a paleomagnetic secular variation record (see Supplementary Figure 1). The uppermost

203   sediment (15 m) spans the past 8 cal ka BP (20 AMS ^{14}C dates) with a near-linear

204   sedimentation rate of 2 m ka^{-1}. Core JR51-GC35, located east of MD99-2269 on the NIS

205   (66$^\mathbf{o}$59.96N, 17$^\mathbf{o}$57.66 W, water depth 420 m; Fig 1a) was collected on board the RRS *James*

206   *Clark Ross* in 2000. An age model was constructed by Bendle and Rosell-Melé (2007), based

207   on linear interpolation between 10 AMS ^{14}C dates, of which 8 cover the last 8 cal ka BP (see

208   Supplementary Figure 1). In order to minimize the possible impacts of degradation of

209   biomarkers, sediment material was taken from previously unsampled archived cores stored at

210   4$^\mathbf{o}$C. A recent study by Cabedo-Sanz et al. (2016) suggests that storage of marine sediment

211   cores under such conditions results in little or no degradation of IP$_{25}$ over several years, at

212   least. All sediment samples were freeze-dried and kept in the freezer (-20$^\mathbf{o}$C) prior to

213   extraction.

214

215   *3.2 Laboratory methods*

216

10

217   *3.2.1 Biomarker analyses*

218   Biomarker analyses (IP_{25} and $C_{25:3}$) were performed using methods described previously

219   (Belt et al., 2012, 2015). Briefly, an internal standard (9-octylheptadec-8-ene, 9-OHD, 10 μL;

220   10 μg mL^{-1}) was added to each freeze-dried sediment sample (ca. 2-3 g) to permit

221   quantification. Samples were then extracted using dichloromethane/methanol (3 x 3 mL; 2:1

222   v/v) and ultrasonication. Following removal of the solvent from the combined extracts using

223   nitrogen, the resulting total organic extracts were purified using column chromatography

224   (silica), eluting IP_{25}, $C_{25:3}$ and other hydrocarbons with hexane (6 mL). Non-polar lipid

225   fractions were further separated into saturated and unsaturated hydrocarbons using glass

226   pipettes containing silver ion solid phase extraction material (Supelco Discovery® Ag-Ion).

227   Saturated hydrocarbons were eluted with hexane (1 mL), while unsaturated hydrocarbons

228   (including IP_{25} and $C_{25:3}$) were eluted with acetone (2 mL). All fractions were dried under a

229   stream of nitrogen. Analysis of the partially purified unsaturated hydrocarbon fraction was

230   carried out using gas chromatography-mass spectrometry (GC-MS) and operating conditions

231   were as described previously (Belt et al., 2012). Mass spectrometric analyses were carried out

232   either in total ion current (TIC) or single ion monitoring (SIM) mode. The identification of

233   IP_{25} (Belt et al., 2007) and $C_{25:3}$ (Belt et al., 2000) was based on their characteristic GC

234   retention indices and mass spectra. Quantification of lipids was achieved by comparison of

235   mass spectral responses of selected ions (SIM mode, IP_{25}, *m/z* 350; $C_{25:3}$, *m/z* 346) with those

236   of the internal standard (9-OHD, *m/z* 350) and normalized according to their respective

237   response factors and sediment masses (Belt et al., 2012). Analytical reproducibility was

238   monitored using a standard sediment with known abundances of biomarkers for every 14–16

239   sediment samples extracted (analytical error 4 %, n=31).

240

241   *3.2.2 Planktic foraminifera*

242 Planktic foraminiferal assemblages were counted from the >150 µm sieve fraction at the

243 same horizons as for IP$_{25}$ analysis. We used 2-cm wide subsamples originally prepared for

244 tephra analysis and Mg/Ca stable isotope analyses (Kristjansdottir et al., 2007). In order to

245 achieve a 25-year sampling resolution, we obtained an additional 106 1-cm wide samples

246 from intervening depths. All samples were prepared by wet sieving at 63 µm, 106 µm and

247 150 µm. The original samples had been air dried at 35°C after sieving and stored dry, while

248 the new sample set was not dried. All samples were analyzed for assemblages in distilled

249 water. We wetted the dried samples prior to wet splitting. We split the samples, where

250 necessary, to achieve a count of at least 200 planktic foraminifers. The planktic counts are

251 expressed as percentages of the total planktic foram assemblages. In this paper, we only

252 show data from the two dominant species, *Neogloboquadrina pachyderma* , an arctic species,

253 and *Turborotalita quinqueloba*, a frontal species that is common at the marine arctic front

254 (Johannessen et al., 1994). We do not include any of the rare dextrally coiled aberrant

255 variants of *N. pachyderma* in counts for *N. pachyderma* because these cannot be

256 distinguished visually from *N. incompta* (Darling et al., 2006).

257

258 *3.2.3 Mineralogical (quartz) data*

259 Quantitative X-ray diffraction (qXRD) of sediment data has been used to track the

260 importation of "foreign" minerals onto the NIS (Moros et al., 2006). Quartz is absent in

261 basalt and thus can be used a robust tracer of importation of sediments carried in either

262 icebergs (from Greenland) or in sea ice (from the Arctic Ocean) (Andrews et al., 2009a,b,

263 2014; Andrews and Eberl, 2007; Eiríksson et al., 2000; Moros et al., 2006).

264

265 *3.3 Statistical data treatment*

266   Some downcore (MD99-2269 and JR51-GC35) IP_{25} and quartz data were converted to equi-

267   spaced time series using the software package Analyseries (Paillard et al., 1996). To perform

268   PCA analysis of all proxy data for MD99-2269, weconverted all variables to 50-yr equi-

269   spaced time-series (n=153 observations for each proxy) using AnalySeries (Paillard et al.,

270   1996), then scaled the data metrics to unit variance, and performed a principal component

271   analysis (PCA) using the statistical software R (package "vegan").

272   In order to evaluate estimates for trends in our sea ice proxy data from MD99-2269, and to

273   ascertain whether residuals from these contained any significant century to millennial-scale

274   periodicities, we performed Singular Spectrum Analysis (SSA) and applied the Multi-taper

275   Method (MTM), respectively, using the commercial version of the UCLA toolkit (kSpectra)

276   (Ghil et al., 2002). Regime shifts are described as statistically significant shifts in the mean of

277   a variable over an interval of time (Rodionov, 2004,2006). The Excel^{TM} macro provided at:

278   www.bering-climate.noaa.gov/regimes/ was used to examine the mean IP_{25} data in MD99-

279   2269. The results will vary depending on the length of the sliding window that is selected to

280   compute differences in averages "before" and "after" each time-step.

281

282   **4 – Results**

283   *4.1 B997- surface sediments*

284   30 surface sediments from SW to N Iceland were analysed for the sea ice biomarker IP_{25}. IP_{25}

285   was present in 17 samples and absent (or below the limit of detection) in the remaining 13.

286   All of the IP_{25}-containing samples were from locations in the N and NW part of the region

287   with higher concentrations found in the northern sites (Fig. 2a). In contrast, IP_{25} was not

288   detected in sediments from the W and SW locations (Fig 2a), consistent with ice-free

289   conditions reported in observational sea ice records (e.g. Ogilvie and Jónsdóttir, 2000).

290   Importantly, the quartz weight % data in the same samples (Andrews and Eberl, 2007)

291   showed a very similar distribution to that of IP_{25} across the sampling region (Fig 2b). Further,

292   the occurrence of the phytoplankton biomarker $C_{25:3}$ also appeared to be confined to the

293   sampling sites in the N and NW regions (Fig. 2c) with a similar distribution to those of IP_{25}

294   and quartz (Fig. 2a,b). In contrast, $C_{25:3}$ was absent, or below the limit of detection, in

295   sediment from the W and SW sampling sites. All surface sediment data can be found in

296   Supplementary Table 1.

297

298   *4.2 Core MD99-2269*

299   In total, 311 and 242 downcore sediment samples were analysed from core MD99-2269 for

300   biomarker content (IP_{25} and $C_{25:3}$) and planktic foraminifera counts (*N. pachyderma* and *T.*

301   *quinqeloba*), respectively (Data can be found in Supplementary Tables 2 and 3). IP_{25} was

302   present in 281 samples and absent (or below the limit of detection) in the remaining 30. The

303   absence of IP_{25}, however, was mainly limited to the early Holocene part of the record with no

304   IP_{25} detected from ca 8 to 7.4 cal ka BP and only intermittently from ca 7.4 to 6.8 cal ka BP,

305   with very low concentration (Fig. 3a). The first continuous occurrence of IP_{25} began at ca 6.8

306   cal ka BP, although concentrations remained relatively low until ca 5.5 cal ka BP, after

307   which, IP_{25} abundances rose steadily to reach their mean value for the record ca 5 cal ka BP,

308   and then further, until ca 4 cal ka BP, apart from a small depletion at ca. 4.4 cal ka BP. The

309   first continuous occurrence of IP_{25} above the mean value was observed at ca 4.3 cal ka BP, at

310   which point, its concentration increased slightly, before remaining relatively stable (although

311   with some fluctuations) up to ca 1.5 cal ka BP. Superimposed on this generally increasing

312   trend, progressive regime shifts to higher concentrations were observed at ca 5.0, 4.3, 3.8,

313   2.7, 1.5, 0.7, 0.4 cal ka BP, although the clearest of these only occurred at ca. 3.8 cal ka BP

314   and afterwards. Highest IP_{25} values occurred at ca 0.1 cal ka BP (Fig. 3), while some slight

14

315   negative deviations from the general trend were observed between ca 2.3 to 1.5 cal ka BP and

316   from ca 1.1 to 0.7 cal ka BP.

317

318   The quartz profile exhibited the same overall trend as IP_{25}, with a general increase from ca

319   8.0 cal ka BP to present, interrupted by a number of short-term variations; however, these did

320   not always coincide with those observed for IP_{25}. Further, the 25 yr equi-spaced time-series

321   (n = 308) from 8 to 0.3 cal ka BP exhibited correlations between the original and equi-spaced

322   values of 0.98 and 0.97 for IP_{25} and quartz, respectively, while a linear regression analysis

323   between both proxies gave a correlation coefficient (R^2) of 0.74 (p = 2 x 10^{-6}), suggesting a

324   strong positive relationship between them.

325

326   In contrast to IP_{25}, the concentration of the phytoplankton biomarker $C_{25:3}$ showed a different

327   profile (only absent in 7 samples), with relatively low concentration during the early

328   Holocene (ca 8 to 6 cal ka BP), generally higher abundance during the mid-Holocene (up to

329   ca 3.5 cal ka BP) before returning to lower concentration during the late Holocene and

330   towards the present (Fig 7c).

331

332   Variations in the percentages of the two most abundant planktonic foraminiferal species, *N.*

333   *pachyderma* and *T. quinqueloba*, covary strongly (Fig. 4). *T. quinqueloba* is the dominant

334   species in the early Holocene, rising in abundance between 8 to 5.4 cal ka BP before

335   declining between 5.4 and 3.4 cal ka BP (Fig. 4a). Between 3 and 1.5 cal ka BP, *T.*

336   *quinqueloba* rises to high and variable percentages, only to decline to very low abundances

337   from 1.5 cal ka BP to modern. *N. pachyderma* abundances maintain a steady background

338   value of ca 30% at the beginning of the record, before rising ca 4.4 cal ka BP. *N. pachyderma*

339   strongly dominates the assemblages (70–90%) after 1.4 cal ka BP (Fig. 4b).

340

341   *4.3. Core JR51-GC35*

342   Compared to that of MD99-2269, a lower resolution IP_{25} record was obtained for core JR51-

343   GC35, with an analysis from 90 downcore sediments covering every ca 4 cm, representing a

344   temporal resolution of ca 100 yr (Data can be found in Supplementary Table 4). IP_{25} could be

345   quantified in 83 out of the 90 samples with all absences occurring prior to ca 6 cal ka BP. The

346   temporal profile for IP_{25} showed the same general trend as observed for MD99-2269 (Fig. 3),

347   with low IP_{25} during the early-mid Holocene, increasing concentrations during the late

348   Holocene and a final decrease towards the present. Interestingly, IP_{25} concentrations in JR51-

349   GC35 were consistently lower than in MD99-2269 throughout the record even though the site

350   is somewhat closer to the average sea ice edge (AD1870-1920). Consistent with the findings

351   for MD99-2269, when the visually similar IP_{25} and quartz profiles were transformed to 100-

352   yr equi-spaced time-series (n = 78; correlation between the original and 100 yr equi-spaced

353   data = 0.98 and 0.96 for IP_{25} and quartz, respectively), a strong coefficient of correlation (R^2

354   = 0.66; p = 3 x 10^{-6}) was also obtained. Finally, the two drift ice proxies were also strongly

355   correlated between the core sites. Thus, correlations between MD99-2269 and JR51-GC35 of

356   R = 0.91 and R = 0.77 were found for IP_{25} and quartz, respectively.

357

358   **5 – Discussion**

359

360   *5.1 IP_{25} as a robust proxy for drift ice*

361   Earlier palaeoenvironmental investigations on the NIS have focused on a variety of proxy-

362   based sea ice (de Vernal et al., 2013b; Moros et al., 2006; Solignac et al., 2006), sea surface

363   temperature (SST) (Andersen et al., 2004b; de Vernal et al., 2013b; Justwan et al., 2008;

364   Solignac et al., 2006; Bendle and Rosell-Melé., 2007; Sicre et al., 2008) and bottom water

365   temperature reconstructions (Giraudeau et al., 2004; Kristjánsdóttir et al., 2007); however, a

16

366 number of disparities exist between them. For example, other than divergence in some SST

367 records (Justwan et al., 2008; Kristjansdottir et al., in press), a monotonic increase in sea ice

368 diagnostic diatoms, as well as other Arctic- and Greenland-diagnostic diatoms from 5 ka BP

369 to at least 1900 AD (Justwan et al., 2008), suggest increased export of Arctic Ocean water

370 and sea ice, particularly over the last ca 2 ka BP, which is supported by the irregular increase

371 in quartz IRD after ca 5 ka BP (Moros et al., 2006). In contrast, a very different sea ice

372 scenario, based on modern analogue treatment (MAT) of dinocyst distributions in MD99-

373 2269/B997-327, reconstructs enhanced sea ice during the early Holocene compared to the

374 late Holocene (de Vernal et al., 2013b; Solignac et al., 2006). Such disparities between

375 dinocyst and other sea ice proxies may reflect, in part, the challenges of establishing robust

376 proxy-sea ice relationships (de Vernal et al., 2013c).

377

378 Previous IP$_{25}$-based sea ice studies for Iceland only span the last two millennia (Andrews et

379 al., 2009a; Axford et al., 2011; Massé et al., 2008; Sicre et al., 2013), with interpretations

380 reliant on the original comparisons by Massé et al. (2008) between IP$_{25}$ abundances in marine

381 core MD99-2275 (NIS) and documentary sea ice records. In order to further establish the use

382 of IP$_{25}$ as a drift ice proxy for N and W Iceland, therefore, we first assessed the spatial

383 distribution of IP$_{25}$ in surface sediments from the region for the first time, and also compared

384 the last millennium components of our new IP$_{25}$ records in MD99-2269 and JR51-GC35 with

385 previous IP$_{25}$ studies covering the past ca 1.2 ka BP, together with documentary sea ice

386 records for the last ca 0.9 cal ka BP.

387

388 The suite of modern surface sediments (B997 cruise) showed that IP$_{25}$ was absent in

389 sediments from W and S Iceland (Fig. 2a), which represent locations that are dominated by

390 ice-free Atlantic waters (Fig. 1), but was common in surface sediment on the NIS, where ice-

17

391   bearing Arctic water masses infringe on surface waters (Fig. 1). Furthermore, since sea ice

392   does not generally form *in situ* around Iceland, the presence of IP_{25} in modern sediments

393   strongly implies that this biomarker represents a signature of drift sea ice and, therefore, a

394   means of tracking sea ice export from the Arctic Ocean. It is also significant that the

395   distribution pattern of IP_{25} closely resembles that of quartz (Fig. 2b), whose presence in

396   sediments around Iceland has also been proposed as a drift ice proxy (e.g. Andrews and

397   Eberl, 2007; Andrews et al., 2009b; Eiríksson et al., 2000; Moros et al., 2006). In addition,

398   the observation of the phytoplankton lipid $C_{25:3}$ in surface sediments from regions

399   experiencing periodic drift ice cover, lends further support to previous suggestions that this

400   biomarker, when identified in polar and sub-polar settings, provides proxy evidence for open

401   water conditions proximal to melting sea ice (Belt et al., 2008, 2015; Massé et al., 2011).

402

403   Next, we compared the IP_{25} profiles spanning the last ca 1.2 cal ka BP in MD99-2269 and

404   JR51-GC35 to previously published IP_{25} records and historical reports of sea ice conditions.

405   Historical records of varying reliability of sea ice conditions from Iceland extend to ca 1 ka

406   BP (Björnsson, 1969; Koch, 1945) and several studies have attempted to demonsrate the

407   relationship between climate and sea ice in the last few centuries (Ogilvie et al., 2000;

408   Ogilvie and Jónsdóttir, 2000; Ogilvie and Jónsson, 2001). Further, the Koch index represents

409   the sea ice extent observed near to the Iceland coasts (Koch, 1945) and a revised version of

410   the Koch index of sea ice cover has been published by Wallevik and Sigurjonsson (1998)

411   (Fig. 5e). From an IP_{25} perspective, Massé et al. (2008) demonstrated that IP_{25} abundances in

412   core MD99-2275 (Fig. 5d), 135 km east of MD99-2269 (Fig. 1a), were very well correlated

413   to these documented sea ice records during the last ca 1 ka (Fig. 5e) and a subsequent study

414   by Andrews et al. (2009a), carried out on a core from the NW Icelandic Shelf (MD99-

415   2263;Fig. 1a), showed a similar IP_{25} profile (Fig. 5c). The current study complements these

416   existing data with IP_{25} profiles from two additional locations on the NIS, both of which show

417   generally good agreement with the previous studies (Fig. 5), especially on a multi-centennial

418   scale. As such, the Little Ice Age (LIA), a widespread cooling period that lasted ca AD 1300–

419   1900 (Jones and Mann, 2004), is clearly recorded in all records across the NIS, suggesting

420   periods of high Arctic Ocean sea ice export and colder summers. In contrast, during the

421   preceding Medieval Warm Period (MWP, ca 1 to 0.7 cal ka BP/ AD 900 to 1200), IP_{25}

422   abundances were lower than during the LIA in all cores (Fig. 5). At higher resolution,

423   increased sea ice observed in the Koch index, especially ca AD 1200 to 1300 are less evident

424   in the IP_{25} records, possibly as a consequence of some mis-matches in temporal sampling (the

425   Koch index is not continuous) or differences between the observational and core locations.

426   However, on a centennial scale, Massé et al. (2008) demonstrated a coherent relationship

427   between IP_{25} abundances, the observational sea ice record and mean northern hemisphere

428   temperatures.

429

430   In summary, the close agreement between IP_{25} (and quartz) content in surface sediments from

431   regions around Iceland reflecting contrasting modern sea ice cover, together with the

432   consistent alignment between IP_{25} profiles in four downcore records and the documented sea

433   ice record during the last ca. 1 ka, provides a convincing case for the use of the IP_{25}

434   biomarker to record changes in drift ice on the NIS in relatively modern and older (e.g.

435   Holocene) sediments.

436

437   *5.2 Reconstruction of palaeoenvironmental conditions during the Holocene*

438   This study represents the first comparison between IP_{25} and quartz from a high-resolution

439   Holocene record on the NIS. Visual inspection and statistical treatment of equi-spaced time

440   series of the IP_{25} and quartz profiles for the MD99-2269 and JR51-GC35 cores (Fig. 3) both

19

441   suggest a similar trend between the two proxies, with low values during the early mid

442   Holocene (ca 8–5.5 cal ka BP) and a mainly unidirectional, but irregular, increase towards the

443   late Holocene (ca 5.5–0 cal ka BP). However, the IP_{25} and quartz concentrations were

444   consistently higher in MD99-2269 compared to those in JR51-GC35, indicative of more drift

445   ice having being delivered to the western region of the NIS (i.e. MD99-2269 area) compared

446   to the eastern part (i.e. JR51-GC35). Although some quartz may also have been deposited

447   from icebergs originating from E/NE Greenland (e.g. Andrews and Eberl, 2007), the close

448   correlation between IP_{25} and quartz in MD99-2269 and JR51-GC35 might indicate that the

449   quartz is mainly derived from sea ice originating on the shallow Arctic Ocean shelves. On the

450   other hand, the potential for some quartz to be delivered as ice-rafted debris from melting

451   icebergs (Andrews et al., 2014) provides a potential explanation for some of the out-of-phase

452   behavior between the quartz and IP_{25} records, most notably between ca 7.0 and 5.0 cal ka BP.

453   In general, however, deviations in the overall IP_{25} profile are reflected in the quartz data.

454

455   In order to better interpret the IP_{25} and quartz data, and to provide further context to the

456   changing environmental conditions on the NIS throughout the Holocene, we expand the

457   Kristjansdottir et al. (in press) analysis of proxy data from MD99-2269 to include the

458   biomarkers IP_{25} and $C_{25:3}$ and planktic foraminifera assemblages (*N. pachyderma* and *T.*

459   *quinqueloba*). Also from MD99-2269, we include two SST reconstructions based on diatoms

460   (Justwan et al., 2008) and the alkenone index $U^{K'}_{37}$ (Kristjansdottir et al., in press), biogenic

461   carbonate (Giraudeau et al., 2004), and quartz data (Moros et al., 2006). PCA of the

462   normalized scores indicated that the first PCA explained 51 % of the variance and the second

463   PCA added a further 24 %. Three main groupings are evident from this analysis (Fig. 6). Not

464   surprisingly, given the good positive correlation between the IP_{25} and quartz profiles, both

465   sea ice proxies were closely grouped in the PCA, while the cold polar water species *N.*

20

466   *pachyderma* also falls within this category, consistent with a strong association with polar

467   surface waters proximal to sea ice (Bé and Tolderlund, 1971; Johannessen et al., 1994). In

468   addition, the loadings of SST proxies fall within a further well-defined cluster (Fig. 6), while

469   biogenic carbonate and the biomarker $C_{25:3}$ are grouped into a third category, probably related

470   to surface water productivity. Indeed, biogenic carbonate produced by coccoliths likely

471   represents a signal of nutrient-rich Atlantic water, although the highest values in this region

472   are normally associated with the IC submerged beneath a shallow layer of fresh and cold

473   polar water (Giraudeau et al., 2004). In this setting, the biomarker $C_{25:3}$ is probably

474   biosynthesized by certain planktic diatoms within the genera *Rhizosolenia* and *Pleurosigma*

475   (Belt et al., 2000; Rowland et al., 2001) residing in surface or near-surface waters. Certainly,

476   this biomarker, when identified in Arctic and Antarctic sediments, has a stable isotopic

477   signature ($\delta^{13}C$ ca -35 to -40 ‰) consistent with a polar phytoplanktonic origin and has

478   recently been identified in elevated abundances in Barents Sea sediments underlying seasonal

479   sea ice cover, and in surface waters off East Antarctica proximal to the marginal ice zone

480   (Belt et al., 2008, 2015; Belt and Müller, 2013; Massé et al., 2011; Smik et al., 2015).

481   Although the drift ice conditions on the NIS are somewhat different to either of these settings,

482   increased production of $C_{25:3}$ appears to be associated with nutrient-fed cold surface waters

483   experiencing periodic drift ice (Fig. 2c). The subpolar foraminifera species *T. quinqueloba*,

484   used as an indicator for the presence of warm Atlantic water in proximity to the marine Arctic

485   Front, is also clustered within the productivity grouping (Fig. 6). In combination, therefore,

486   biogenic carbonate, $C_{25:3}$ and *T. quinqueloba* proxies should provide an indication of open

487   water conditions and related surface/sub-surface water productivity on the NIS. Finally,

488   Kristjansdottir et al. (in press) applied a statistical treatment to a suite of SST (alkenone and

489   Mg/Ca), mineralogical and stable light isotope (planktic and benthic forams) data for MD99-

490   2269 to show that the Holocene paleoceanographic evolution on the NIS could be classified

491   according to three temporal divisions (viz. ca 8.0–6.3 ka BP, 6.3–4.0 ka BP and 4.0 ka BP–

492   present). These boundaries reflect regional climate and are offset from the suggested global

493   boundaries (Walker et al., 2012) and we use these regionally defined intervals as the basis for

494   our interpretations, albeit with a slight shift in the later boundary (to ca. 3.3 ka BP) to

495   accommodate the new biomarker and foraminifera data. The interpretations of our new proxy

496   data are, therefore, as follows:

497

498   *5.2.1 Early mid Holocene (8–6.2 cal ka BP)*

499   The early mid Holocene (ca 8–6.2 cal ka BP) is characterized as an interval of ice-free (or

500   nearly ice-free) conditions as shown by absent (or very low) IP_{25} concentration (Fig. 7h) and

501   low quartz content in MD99-2269 (Fig. 7g, Moros et al., 2006). A similar conclusion can be

502   reached from the corresponding IP_{25} and quartz records in core JR51-GC35 (Fig. 3b). In

503   addition, the percentages of the cold polar water foraminifera species *N. pachyderma* were

504   also very low during this period (Fig. 7f), whereas the Atlantic water/sub-polar species *T.*

505   *quinqueloba* was relatively abundant (Fig. 7d), reflecting the greater influence of the warm

506   IC compared to cold polar waters from the EGC on the NIS. Summer SSTs, obtained by

507   diatom transfer functions (Justwan et al., 2008), and alkenone-based ($U^{K'}_{37}$) SST

508   reconstructions (Fig. 3,7e) (Kristjansdottir et al., in press), were also at their highest during

509   this interval, coincident with higher summer insolation (Fig. 7a). This interval likely

510   represents the end of the NIS Holocene Thermal Maximum (HTM) or a relatively warm

511   phase following peak warmth during the HTM; a conclusion consistent with other

512   palaeoclimate reconstructions across the Northern Hemisphere and the study region (e.g.

513   Andersen et al., 2004a; Andrews et al., 2003; Geirsdóttir et al., 2009,2013; Kaufman et al.,

514   2004; Ólafsdóttir et al., 2010). The occurrence of absent/low sea ice conditions during the

515   early mid Holocene in our NIS records has also been observed in several previous studies

516   from other Arctic and sub-Arctic regions including the Canadian Arctic Archipelago (Belt et

517   al., 2010; Vare et al., 2009), the Fram Strait (Müller et al., 2009, 2012), the East Greenland

518   Shelf (Müller et al., 2012) and the Barents Sea (Belt et al., 2015; Berben et al., 2014). In

519   contrast, a dinocyst-based sea ice reconstruction for the NIS indicated longer sea ice extent

520   prior to ca 6.2 cal ka BP (Solignac et al., 2006) even after revision of the modern dinocyst-

521   assemblage transfer function using an updated database (de Vernal et al., 2013b,c). The

522   reason for this difference between the IP_{25} (and quartz) data and the dinocyst-based

523   reconstruction is still not clear at this point and remains a topic of debate. In the meantime,

524   Polyak et al. (2016) and Cabedo-Sanz et al. (2016) have suggested that such differences are

525   likely due to the precise nature of the respective proxy signatures. Thus, Cabedo-Sanz et al.

526   (2016), in particular, point out that dinocyst-based reconstructions yield information

527   regarding sea ice duration – specifically, the number of months of >50% sea ice cover –

528   while IP_{25} provides a more sensitive indicator of spring sea ice conditions. Such nuances

529   may be particularly important for regions of relatively low sea ice cover and less extreme

530   seasonality, as is the case for north Iceland and the west Svalbard margin (Cabedo-Sanz et al.,

531   2016). Finally, biogenic carbonate was also very low during this period (Fig. 7b, Giraudeau et

532   al., 2004), indicating low coccolithophore productivity at this time, while the consistently low

533    $C_{25:3}$ concentration during this interval (Fig. 7c), also suggests a period of reduced

534   phytoplankton productivity, despite higher SSTs (Fig. 7e), likely due to the low/absent sea ice

535   conditions during this interval.

536

537   *5.2.2 Mid-Holocene (6.2–3.3 cal ka BP)*

538   The mid-Holocene was characterised by a gradual increase in drift ice, as indicated by

539   generally parallel enhancements in IP_{25} and quartz in both MD99-2269 and JR51-GC35 (Fig.

540   3; 7g,h). At ca 6.2 cal ka BP, *N. pachyderma* values (Fig. 7f) remained quite low, although

23

541   an increasing trend was observed beginning ca 5 cal ka BP, with an opposing profile for *T.*

542   *quinqueloba* (Fig. 7d). These observations indicate a gradual cooling of surface waters on the

543   NIS during this interval and are further corroborated by decreasing reconstructed SSTs after

544   ca 5 cal ka BP (Fig. 3,7e). Such outcomes are also consistent with observations made

545   previously for the western side of Denmark Strait (Jennings et al., 2011). Despite this

546   cooling, however, Giraudeau et al. (2004) demonstrated enhanced biogenic carbonate in

547   MD99-2269 beginning at ca. 6.5 cal ka BP (Fig. 7b) and attributed this to increased

548   productivity related to strengthening of the water column stratification via increased

549   advection of EGC freshwater to the NIS, which resulted in optimized conditions for blooms

550   of the coccolithophore species *Coccolithus pelagicus*. We also note a sharp increase in the

551     $C_{25:3}$ concentration in MD99-2269 at ca 6.2 cal ka BP, and generally higher $C_{25:3}$

552   concentrations are evident until ca 3.3 cal ka BP (Fig. 7c). Termination of this interval of

553   elevated $C_{25:3}$ coincides with a further increase in IP_{25} concentration and quartz content. We

554   propose a scenario whereby some drift ice reached the area during (still) relatively warm

555   (SST) conditions, resulting in enhanced primary productivity in the upper water column.

556   Interestingly, this observation of highest productivity during the mid-Holocene is in

557   accordance with recent findings from the East Greenland shelf based on planktic and benthic

558   foraminifera (Perner et al., 2015).

559

560   *5.2.3 Late Holocene (3.3 cal ka BP–present)*

561   Our proxy data indicate that the late Holocene can be divided into two sub-intervals. During

562   the first sub-interval (ca 3.3–1.5 cal ka BP), IP_{25} values were more variable than during the

563   mid-Holocene (Fig. 7h), and a similar trend was also observed in the quartz wt% data (Fig.

564   7g), suggesting that increasing, but more variable, drift ice conditions prevailed. Significant

565   short-term temporal variability is also observed in the planktic foraminifera *N. pachyderma*

24

566 and *T. quinqueloba* (Fig. 7d,f). We ascribe this strong co-variance to frequent changes in the

567 influence of polar waters compared to Atlantic waters in proximity to the marine polar front.

568 SSTs also showed some variability, but were at their lowest values for the entire record,

569 especially from ca 3.3 to 2.5 cal ka BP (Fig. 7e). Low alkenone-based SSTs were also evident

570 around this time in JR51-GC35 (Fig. 3). A particularly abrupt transition in the IP_{25} record

571 was recorded in the second half of the record at ca 1.5 cal ka BP, and this was also evident in

572 the other proxies, although to a lesser extent. During this second sub-interval of the late

573 Holocene (ca 1.5–0 cal ka BP), the IP_{25} record exhibited notable increases in concentration

574 towards the present (e.g. ca 0.7 and 0.4 cal ka BP, Fig. 7h, 8e), with highest values for the

575 entire profile recorded during the LIA (ca 0.1–0.6 ka BP). Parallel observations were also

576 evident in the quartz data for MD99-2269 and in the IP_{25} profile for JR51-GC35 (Fig. 3b).

577 Together with highest *N. pachyderma* %, our combined proxy data point to a progressively

578 cooler interval, with increasing influences from cold polar water and drift ice delivered by the

579 EGC, and the EIC, in particular. Interestingly, the identification of step-wise shifts towards

580 colder states aligns well with a recent study off East Greenland, whereby Perner et al. (2105)

581 identified a southward shift of the Subpolar Front (Moros et al., 2012) during the late

582 Holocene, that may have restricted deep convection in the Nordic Seas (e.g. Renssen et al.,

583 2005; Telesiński et al., 2014).

584

585 Increased sea ice delivery to the MD99-2269 site, especially during the second half of the late

586 Holocene is accompanied by decreasing biogenic carbonate (Fig. 7b) and generally very low

587 $C_{25:3}$ concentration (Fig. 7c), with both productivity proxies reaching their lowest values

588 during the LIA (Fig. 7b,c). We interpret these changes as further support for a combination of

589 colder surface temperatures and increased influence of polar waters and drift ice. Indeed,

590 alkenone-based SST reconstructions from the eastern part of the NIS (e.g., JR51-GC35) show

25

591   cooling during the last ca 2 cal ka BP (Bendle and Rosell-Melé, 2007) and, therefore,

592   consistency with the IP_{25} records in JR51-GC35 (Fig. 3b) and the last ca 1 ka in MD99-2275

593   (Fig. 4) (Massé et al., 2008). In contrast, however, SST records reconstructed for MD99-2269

594   based on diatoms (Justwan et al., 2008) and alkenones (Kristjansdottir et al., in press) both

595   show a slight warming trend during the late Holocene (Fig. 7e), as does a more recent

596   alkenone-based SST record for a fjordic setting from NW Iceland (Moossen et al., 2015), all

597   of which appear to be inconsistent with other SST records and with the IP_{25} and quartz sea ice

598   record in MD99-2269 (Fig. 7h) and other North Atlantic regions (e.g. Calvo et al., 2002;

599   Müller et al., 2012; Rasmussen et al., 2012; Risebrobakken et al., 2009; Sarnthein et al.,

600   2003b; Telesiński et al., 2014; Werner et al., 2013) and further afield (McGregor et al., 2015).

601

602   Moossen et al. (2015) attributed the late Holocene upturn in SSTs seen in a fjord record from

603   NW Iceland to a dominant influence of the North Atlantic Oscillation (NAO) in its positive

604   phase during this time, and the same explanation may also be pertinent for MD99-2269.

605   However, this would require that such influences of NAO+ are substantially reduced for the

606   sites further east (JR51-GC35 and the MD99-2275) since these both show long-term cooling.

607   Regardless of the forcing mechanism(s), increased SSTs of the upper 1–2 m of the water

608   column may have been driven by the presence of a thin freshwater lid which restricted

609   mixing with deeper colder water and the supply of nutrients. Potentially, this may have been

610   more important for the MD99-2269 site, compared to JR51-GC35 further east, since our IP_{25}

611   and quartz records both show consistently higher sea ice extent for the former throughout the

612   respective records (Fig. 3). Alternatively, greater seasonal decoupling between sea ice and

613   SST may have been especially relevant during the late Holocene, with colder winters and

614   warmer summers in the western part of the NIS (i.e. MD99-2269) compared to the eastern

615   study sites (i.e. MD99-2275 and JR51-GC35), possibly resulting from a greater influence of

26

616   the IC for the former. Related to this, there may have been a shift in the season(s) that the

617   SST proxies reflect, especially during higher sea ice conditions. Indeed, warmer alkenone

618   SSTs compared to instrumental data were observed for certain cold periods in core MD99-

619   2275 (Sicre et al., 2011), possibly associated with sea ice occurrence. Further, late Holocene

620   alkenone-derived SSTs for NE and SE Newfoundland showed higher SST for the former,

621   despite near year-round cooler temperatures in the instrumental record, an anomaly explained

622   by the presence of drift ice for the NE Newfoundland site which likely caused a delay in the

623   algal bloom to later (and warmer) months compared to the early (cooler) spring bloom for the

624   SE Newfoundland site (Sicre et al., 2014).

625

626   Finally, some SST anomalies may exist in some of the records especially if, for example, the

627   transfer function used for the diatom-derived SST record (Justwan et al., 2008) is too heavily

628   weighted on the North Atlantic taxa and, in any case, there is a clear and consistent (ca 2 ℃)

629   offset between the diatom and alkenone SSTs records for MD99-2269, with both methods

630   providing significant overestimates of SSTs for the modern setting (ca 5 ℃; Fig. 1).

631

632   *5.4 Broader significance*

633   The determination of a long-term and high-resolution sea ice record for the NIS (MD99-

634   2269), which is also consistent with a further sea ice record from further east (JR51-GC35)

635   and with other proxy data, suggest that our outcomes are representative of a broad geographic

636   area. As such, the new findings presented here enable us to add to the understanding of the

637   role of sea ice in Northern Hemisphere Holocene climate evolution, including identification

638   of key climatic events (e.g. onset of Neoglaciation and the LIA) and the coupling between the

639   marine and terrestrial environments.

640

641   *5.4.1 Holocene cooling and sea ice expansion at the onset of Neoglaciation*

642   Previous comparisons between terrestrial and marine proxy records, combined with those

643   from modeling studies, have indicated that Neoglacial cooling began during the mid-

644   Holocene (ca 5 ka). There is, however, no agreed consensus date for the onset of Neoglacial

645   conditions. For example, within the terrestrial realm, a recent regional compilation of [14]C

646   dates performed on ice-edge rooted plants collected from Baffin Island, West Greenland and

647   Svalbard strongly suggests that the onset of Neoglacial cooling occurred shortly after 5 ka

648   (Miller et al., 2013a,b). In the marine environment, previous studies have reported a decrease

649   in Atlantic water inflow after ca 5.5 cal ka BP in Arctic regions influenced by the EGC such

650   as eastern Fram Strait and fjord/shelf areas of Spitsbergen (e.g. Aagaard-Sørensen et al.,

651   2014; Hald et al., 2007; Werner et al., 2013) while, most recently, Perner et al. (2015)

652   identified significant strengthening of the EGC on the central East Greenland shelf at ca 4.5

653   cal ka BP, with an inference of enhanced sea ice export. Climate modelling also suggests that

654   sea ice is an important amplifier of summer cooling and contributes to persistent cold

655   conditions (Schleussner and Feulner, 2013). Consistent with these studies, recent proxy-based

656   reconstructions of sea ice in the northern North Atlantic have demonstrated strong

657   associations between enhanced sea ice conditions and Holocene cooling (e.g. Fahl and Stein,

658   2012; Koç et al., 1993; Müller et al., 2012; Werner et al., 2013). Thus, based on IP_{25} and

659   IRD data, Müller et al. (2012) showed that a significant expansion of sea ice and icebergs

660   occurred during the Neoglacial in the Fram Strait and their findings were supported by the

661   analysis of the polar planktic foraminifer species *N. pachyderma* in the same record (Werner

662   et al., 2013). Further, analysis of remnant diatoms in a N to S core transect in the Greenland,

663   Iceland and Norwegian seas showed a cooling trend and a southeastward spread of the sea ice

664   margin in polar surface waters and of the polar and arctic fronts after ca 5.5 cal ka BP (Koç et

665   al., 1993).

666

667   In addition to the these long-term trends, intermittent advances of Northern Hemisphere ice

668   sheets and glaciers have also been recorded, of which the LIA was the most extreme multi-

669   centennial departure (Geirsdóttir et al., 2013; Miller et al., 2010). As such, regional feedbacks

670   such as volcanic eruptions likely modulate climatic signatures, such as sea ice, that reflect

671   primary insolation forcing (Geirsdóttir et al., 2013; Miller et al., 2012). Indeed, relatively

672   small changes in insolation during the last ca 1.5 ka compared to the early and mid Holocene

673   (Fig. 7a), likely requires the influence of additional forcing mechanisms such as explosive

674   volcanism (McGregor et al., 2015) to explain the late Holocene cooling trend. Climate

675   modelling experiments also suggest that persistent summer cold could be explained by a

676   series of paced eruptions that initiated a shelf-sustaining expansion of Arctic Ocean sea ice

677   that persisted for centuries after the volcanic aerosols were removed from the atmosphere

678   (Miller et al., 2012; Zhong et al., 2011), while Sicre et al. (2013) recently demonstrated the

679   likely coupling between volcanic eruptions and nearby sea ice on the NIS, albeit on a fairly

680   reduced timescale (AD 1000–1400 yr).

681

682   Turning our attention to the MD99-2269 record, the increase in IP_{25} to it mean value ca 5 cal

683   ka BP and continually above this after ca 4.3 cal ka BP (Fig. 8d), marks a significant change

684   in sea ice export, although more abrupt increases are clearer in the later part of the record. A

685   sustained period of elevated IP_{25} and a generally increasing trend throughout the remainder of

686   the Holocene, with highest concentrations reached ca 0.1 cal ka BP, point to overall enhanced

687   sea ice export after ca. 5 cal ka BP, which culminated during the LIA. This general trend of

688   increasing sea ice found in both records (MD99-2269 and JR51-GC35) aligns well with other

689   IP_{25}-based sea ice reconstructions for the Fram Strait and central East Greenland (Fig. 8b, 8c)

690   (Müller et al., 2012) and other inferences of sea ice change in the northern North Atlantic

691   (Koç et al., 1993; Telesiński et al., 2014; Werner et al., 2013) and northern Greenland

692   (Funder et al., 2011). In addition, maximum IP_{25} concentrations during the LIA have been

693   observed previously in other north Atlantic marine records from Fram Strait and the East

694   Greenland shelf (Müller et al., 2012) and from other sites around N Iceland (Andrews et al.,

695   2009a; Massé et al., 2008). Our biomarker observations are also supported by the quartz data

696   from MD99-2269 (Fig. 8b, Moros et al., 2006) and confirm suggestions made previously by

697   Perner et al. (2015) based on analysis of sediment core PS2641-4 from the central East

698   Greenland shelf, whereby a southeasterly shift in the position of the polar front, reflecting an

699   increase in the EGC, was accompanied by enhanced sea ice export during the Neoglaciation

700   after ca 4.5 cal ka BP. In addition, IRD records for East Greenland are also enhanced during

701   the Holocene, and especially in the last ca 5 cal ka BP (Andrews et al., 1997). On the other

702   hand, although Müller et al. (2012) identified IP_{25} in PS2641-4 throughout the Holocene (Fig.

703   8c), increased abundances were only observed during the last ca 1 ka, which was attributed to

704   a possible easterly broadening of the EGC as a result of enhanced ice export, without

705   necessarily impacting on conditions proximal to the East Greenland coast.

706

707   Superimposed on the longer-term trend seen during the mid-late Holocene, we also observed

708   pronounced millennial-scale positive IP_{25} regime shifts (cold-phases) in MD99-2269 mainly

709   at ca 3.8, 2.7, 1.5, 0.7 and 0.4 cal ka BP (LIA) (Fig. 3,8e) which have been recorded in other

710   EGC-influenced regions (Moros et al., 2012; Perner et al., 2015) and in the same record at ca

711   3.0 and 0.2–0.6 cal ka BP (LIA) (Giraudeau et al., 2004). In addition, a pronounced negative

712   IP_{25} deviation is seen from ca 2.3 to 1.5 cal ka BP which coincides with an interval of relative

713   warming seen in many records from the northern North Atlantic (Giraudeau et al., 2004;

714   Jennings et al., 2002; Moros et al., 2012; Risebrobakken et al., 2003; Sarnthein et al., 2003a)

715   and previously ascribed to the Roman Warm Period (Perner et al., 2015), during which there

716   was likely a temporary strengthening of the North Atlantic Drift and NAC.

717

718   A previous study by Ólafsdóttir et al. (2013) showed that Icelandic climate has also been

719   sensitive to the state of both the North Atlantic Oscillation and Atlantic Meridional

720   Overturning (Andrews and Jennings, 2014) through the past 3 ka, at least, while Miller et al.

721   (2012) suggested that it was also likely strongly impacted by sea ice export from the Arctic

722   Ocean, so the latter is also supported by our IP_{25}-derived sea ice data (Fig. 8e). Certainly, for

723   increased sea ice to be recorded as far south as the NIS requires a substantial expansion of the

724   entire Arctic Ocean pack, a weakening of the NAC, and altered surface water characteristics

725   in the Atlantic subpolar gyre, with potential further impacts, downstream. The coherence

726   between the MD99-2269 record for the NIS and those presented previously for Fram Strait

727   and the East Greenland shelf (Müller et al., 2012) certainly endorses this view.

728

729   *5.4.2. Marine and terrestrial coupling*

730   From a local perspective, the proximity of the study site to Iceland and the existence of a

731   composite terrestrial record (Geirsdóttir et al., 2013) provide an additional opportunity to

732   examine the coupling between marine and terrestrial settings during the Holocene.

733   Previously, Larsen et al. (2011) showed that the ca 1 ka IP_{25} record from MD99-2275 (Massé

734   et al., 2008) aligned closely with the reconstructed dimensions of the Langjökull ice cap,

735   suggesting a close link between terrestrial summer temperatures and changes in sea ice cover

736   in the nearby ocean. Sicre et al. (2013) demonstrated a (lagged) coupling between volcanic

737   eruptions, SSTs and nearby sea ice from a site slightly further north (MD99-2273; Fig. 1a),

738   during the interval AD 1000–1400 yr. In this study, we extend these previous investigations

739   by comparison of the Holocene IP_{25} and quartz data from the MD99-2269 marine record with

31

740   a terrestrial record based on a composite multiproxy (e.g., biogenic silica, TOC, $\delta^{13}C$, C/N.

741   sediment density, magnetic susceptibility) summer climate reconstruction from two Icelandic

742   lakes (Hvitarvatn/Haukadalsvatn) (Geirsdóttir et al., 2013). Interestingly, both the marine (sea

743   ice) and terrestrial records follow the regional decrease in summer insolation (Fig. 8a) as a

744   first-order trend towards cooler summers, with a threshold change in the terrestrial record ca

745   5.5 cal ka BP, previously ascribed to the onset of the Neoglaciation (Fig. 8e) (Geirsdóttir et

746   al., 2013), aligning well with the first sustained increase in the IP_{25} record (ca 5 cal ka BP). In

747   addition, after ca 4 cal ka BP, virtually all IP_{25}, quartz and terrestrial record values were

748   above, and increased beyond, their mean Holocene values (Fig. 8), suggesting progressively

749   cooler summers, increased sea ice, and thus a likely synergy between them. In addition to

750   these general (insolation-driven) changes, an abrupt cooling at ca 5.0 cal ka BP, followed by

751   further regime shifts (step coolings) at ca. 4.2, 3.0, 1.5 and 0.7 cal ka BP were observed

752   previously in the lacustrine composite (Fig. 8f) some of which might be ascribed to the

753   impacts of local volcanic activity (Geirsdóttir et al., 2013). Although the magnitude of the

754   respective changes in the terrestrial and marine records may not be the same, it is important

755   to note that paleomagnetic secular variation data confirm that the Icelandic lake

756   (Hvitarvatn/Haukadalsvatn) (Geirsdóttir et al., 2013) and marine (MD99-2269) records are

757   highly synchronized (Geirsdóttir et al., 2013) so are temporally comparable. In any case,

758   some clear and positive departures from the generally trend in the IP_{25} record are observed at

759   ca 4.2 and 2.6 cal ka BP, and most notably at ca 1.5 cal ka BP and during the LIA (ca 0.4 cal

760   ka BP), supporting the notion of significant coupling between the marine and terrestrial

761   systems.

762

763   *5.4.3. Drift ice periodicity*

764 The high resolution of our data for MD99-2269 over the last ca 8 ka BP has enabled us to

765 identify certain periodicities in the drift ice proxy data using spectral analysis. In the first

766 instance, SSA of the 30-yr equi-spaced data indicated that statistically significant trends (first

767 SSA component) in both IP_{25} and quartz data existed, with 76 % and 82 % of the variance

768 explained by each component, respectively. Significant periodicities in the detrended time-

769 series were detected using the MTM, with confidence levels of 95 and 99% relative to

770 estimated red-noise background (Mann and Lees, 1996). The spectral features for both drift

771 ice proxies are shown in Fig. 9. MTM analysis of the detrended IP_{25} series produced

772 significant periods (95–99 % confidence interval) of 213, 275, and 1024 yr (Fig. 9a), while

773 the corresponding quartz series showed three significant periodicities at 156, 208 and 334 yr

774 (Fig. 9b; 95 % confidence interval). Interestingly, the 1024 yr period recorded in the IP_{25}

775 record (Fig. 9a) compares well with a similar periodicity (ca 1000 yr) from the Holocene

776 $\delta^{18}O$ GISP2 ice core record (Stuiver et al., 1995), while Chapman and Shackleton (2000)

777 provided further evidence for a ca 1000 yr cyclicity based on a lightness profile in a sediment

778 core record from Gardar Drift (SW Iceland), and suggested an interconnection between

779 atmospheric and oceanic variability. As such, our IP_{25} data provide further evidence for

780 coupling between the atmosphere and marine environment. In addition, the MTM coherence

781 analysis performed on the IP_{25} and quartz detrended series indicated shared periodicities

782 between these drift ice proxies of 205 and 232 yr (significance = 95 %). Thus, spectral

783 analysis performed on the individual and combined drift ice proxies provide strong evidence

784 for at least one periodicity of ca 200–230 yr. Interestingly, a similar ca 200 yr period

785 oscillation in magnetic properties in MD99-2269 was previously identified by Andrews et al.

786 (2003) and was consistent with the 'Suess' wiggles in $\Delta^{14}C$ that have been detected at a 208

787 yr period in previous analyses of $\Delta^{14}C$ Holocene records (Thomson, 1990). A 200 yr period

33

788   has also been detected in dust measurements from the GISP2 record and was associated with

789   solar variability (Ram and Stolz, 1999).

790

791   **6 – Conclusions**

792   The identification of IP_{25} as a reliable proxy for drift ice for North Iceland has been

793   confirmed based on the analysis of surface sediments from the region and comparison of

794   outcomes with documentary records and other (mineralogical) proxy data. A high-resolution

795   reconstruction of sea ice, productivity, SST and water masses based on new (IP_{25}, $C_{25:3}$,

796   planktic foraminifera) and existing (quartz, alkenone and diatom SST, productivity (biogenic

797   carbonate)) proxy data from marine sediment core MD99-2269 indicates a three-interval

798   Holocene climate record consistent with a previous study (Kristjansdottir et al., in press).

799   Thus, the early mid Holocene (ca 8–6.2 cal ka BP) was characterized by relatively low drift

800   ice, low primary productivity and relatively high SSTs. During the mid-Holocene (ca 6.2–3.3

801   cal ka BP) drift ice increased progressively as SSTs decreased, and primary productivity was

802   also enhanced during this period. A period of sustained increase in drift ice began ca 5.0–4.4

803   cal ka BP, coincident with the onset of Neoglaciation, with further increases into the late

804   Holocene (ca 3.3 cal ka BP to present), culminating in maximum sea ice during the LIA. In

805   addition to these general trends, the IP_{25} record shows some step shifts towards enhanced

806   drift ice conditions ca 3.8, 2.7, 1.5, 0.7 and 0.4 cal ka BP that have been also recorded in

807   other EGC-influenced regions. Some of these positive departures, especially those at ca 1.5

808   and 0.7 cal ka BP, coincide with abrupt cooling recorded in an Icelandic lacustrine

809   temperature composite, suggesting significant coupling between the marine and terrestrial

810   systems. The association of sea ice to the broader climate system is further evidenced by the

811   identification of statistically significant periodicities in the drift ice data (MD99-2269) of ca

812   1000 yr (IP_{25}) and ca 200–230 yr (IP_{25} and quartz), which have counterparts in previous

34

813   studies concerning atmospheric and oceanic variability (Chapman and Shackleton, 2000;

814   Stuiver et al., 1995) and solar forcing (Ram and Stolz, 1999). Overall, therefore, our

815   combined proxy data suggest that the NIS experienced a sustained increase in sea ice during

816   the Holocene, especially after ca 5 ka BP, but with some overprinting due to shorter-term

817   enhancements/reductions, possibly attributed to a combination of volcanic and solar cycle

818   forcings.

819

820   **7 – Acknowledgements**

8 – References

829

830 Aagaard-Sørensen, S., Husum, K., Hald, M., Marchitto, T., Godtliebsen, F., 2014. Sub sea
831 surface temperatures in the Polar North Atlantic during the Holocene: Planktic foraminiferal
832 Mg/Ca temperature reconstructions. The Holocene 24, 93–103.

833 Aagaard, K., Coachman, L.K., 1968. The East Greenland Current north of Denmark Strait:
834 Part I. Arctic 21, 181–200.

835 Andersen, C., Koç, N., Jennings, A., Andrews, J.T., 2004a. Nonuniform response of the
836 major surface currents in the Nordic Seas to insolation forcing: Implications for the Holocene
837 climate variability. Paleoceanography 19, PA2003.

838 Andersen, C., Koç, N., Moros, M., 2004b. A highly unstable Holocene climate in the
839 subpolar North Atlantic: evidence from diatoms. Quaternary Science Reviews 23, 2155–
840 2166.

841 Andrews, J.T., Smith, L.M., Preston, R., Cooper, T., Jennings, A.E., 1997. Spatial and
842 temporal patterns of iceberg rafting (IRD) along the East Greenland margin, ca. 68˚N, over
843 the last 14 cal. ka. Journal of Quaternary Science 12, 1–13.

844 Andrews, J.T., Hardadottir, J., Stoner, J.S., Mann, M.E., Kristjansdottir, G.B., Koc, N., 2003.
845 Decadal to millennial-scale periodicities in North Iceland shelf sediments over the last 12 000
846 cal yr: long-term North Atlantic oceanographic variability and solar forcing. Earth and
847 Planetary Science Letters 210, 453–465.

848 Andrews, J.T., Eberl, D.D., 2007. Quantitative mineralogy of surface sediments on the
849 Iceland shelf, and application to down-core studies of Holocene ice-rafted sediments. Journal
850 of Sedimentary Research 77, 469–479.

851 Andrews, J.T., 2009. Seeking a Holocene drift ice proxy: non-clay mineral variations from
852 the SW to N-central Iceland shelf: trends, regime shifts, and periodicities. Journal of
853 Quaternary Science 24, 664–676.

854 Andrews, J.T., Belt, S.T., Olafsdottir, S., Massé, G., Vare, L.L., 2009a. Sea ice and marine
855 climate variability for NW Iceland/Denmark Strait over the last 2000 cal. yr BP. The
856 Holocene 19, 775–784.

857 Andrews, J.T., Darby, D., Eberle, D., Jennings, A.E., Moros, M., Ogilvie, A., 2009b. A
858 robust, multisite Holocene history of drift ice off northern Iceland: implications for North
859 Atlantic climate. The Holocene 19, 71–77.

860 Andrews, J.T., Bigg, G.R., Wilton, D.J., 2014. Holocene ice-rafting and sediment transport
861 from the glaciated margin of east Greenland (67–70° N) to the N Iceland shelves: detecting
862 and modelling changing sediment sources. Quaternary Science Reviews 91, 204–217.

863 Andrews, J.T., Jennings, A.E., 2014. Multidecadal to millennial marine climate oscillations
864 across the Denmark Strait (~ 66 N) over the last 2000 cal yr BP. Climate of the Past 10, 325–
865 343.

866 Axford, Y., Andresen, C.S., Andrews, J.T., Belt, S.T., Geirsdóttir, Á., Massé, G., Miller,
867 G.H., Ólafsdóttir, S., Vare, L.L., 2011. Do paleoclimate proxies agree? A test comparing 19
868 late Holocene climate and sea-ice reconstructions from Icelandic marine and lake sediments.
869 Journal of Quaternary Science 26, 645–656.

870 Bé, A.W., Tolderlund, D.S., 1971. Distribution and ecology of living planktonic foraminifera
871 in surface waters of the Atlantic and Indian Oceans. Cambridge University Press, London.

872 Belkin, I.M., Levitus, S., Antonov, J., Malmberg, S.-A., 1998. "Great salinity anomalies" in
873 the North Atlantic. Progress in Oceanography 41, 1–68.

874 Belkin, I.M., Cornillon, P.C., Sherman, K., 2009. Fronts in large marine ecosystems. Progress
875 in Oceanography 81, 223–236.

876 Belt, S.T., Allard, W.G., Massé, G., Robert, J.-M., Rowland, S.J., 2000. Highly branched
877 isoprenoids (HBIs): identification of the most common and abundant sedimentary isomers.
878 Geochimica et Cosmochimica Acta 64, 3839–3851.

879 Belt, S.T., Massé, G., Rowland, S.J., Poulin, M., Michel, C., LeBlanc, B., 2007. A novel
880 chemical fossil of palaeo sea ice: IP_{25}. Organic Geochemistry 38, 16–27.

881 Belt, S.T., Massé, G., Vare, L.L., Rowland, S.J., Poulin, M., Sicre, M.-A., Sampei, M.,
882 Fortier, L., 2008. Distinctive ^{13}C isotopic signature distinguishes a novel sea ice biomarker in
883 Arctic sediments and sediment traps. Marine Chemistry 112, 158–167.

884 Belt, S.T., Vare, L.L., Massé, G., Manners, H.R., Price, J.C., MacLachlan, S.E., Andrews,
885 J.T., Schmidt, S., 2010. Striking similarities in temporal changes to spring sea ice occurrence
886 across the central Canadian Arctic Archipelago over the last 7000 years. Quaternary Science
887 Reviews 29, 3489–3504.

888 Belt, S.T., Brown, T.A., Navarro Rodriguez, A., Cabedo Sanz, P., Tonkin, A., Ingle, R.,
889 2012. A reproducible method for the extraction, identification and quantification of the Arctic
890 sea ice proxy IP_{25} from marine sediments. Analytical Methods 4, 705–713.

891 Belt, S.T., Brown, T.A., Ringrose, A.E., Cabedo-Sanz, P., Mundy, C.J., Gosselin, M., Poulin,
892 M., 2013. Quantitative measurement of the sea ice diatom biomarker IP_{25} and sterols in
893 Arctic sea ice and underlying sediments: Further considerations for palaeo sea ice
894 reconstrucion. Organic Geochemistry 62, 33–45.

895 Belt, S.T., Müller, J., 2013. The Arctic sea ice biomarker IP_{25}: a review of current
896 understanding, recommendations for future research and applications in palaeo sea ice
897 reconstructions. Quaternary Science Reviews 79, 9–25.

898   Belt, S.T., Cabedo-Sanz, P., Smik, L., Navarro-Rodriguez, A., Berben, S.M., Knies, J.,
899   Husum, K., 2015. Identification of paleo Arctic winter sea ice limits and the marginal ice
900   zone: Optimised biomarker-based reconstructions of late Quaternary Arctic sea ice. Earth and
901   Planetary Science Letters 431, 127–139.

902   Bendle, J.A., Rosell-Melé, A., 2007. High-resolution alkenone sea surface temperature
903   variability on the North Icelandic Shelf: implications for Nordic Seas palaeoclimatic
904   development during the Holocene. The Holocene 17, 9–24.

905   Berben, S.M.P., Husum, K., Cabedo-Sanz, P., Belt, S.T., 2014. Holocene sub centennial
906   evolution of Atlantic water inflow and sea ice distribution in the western Barents Sea.
907   Climate of the Past 10, 181–198.

908   Berger, A., Loutre, M.F., 1991. Insolation values for the climate of the last 10 million years.
909   Quaternary Science Reviews 10, 297–317.

910   Bergthorsson, P., 1969. An estimate of drift ice and temparature in Iceland in 1000 years.
911   Jokull 19, 94–101.

912   Björnsson, H., 1969. Sea ice conditions and the atmospheric circulation north of Iceland.
913   Jokull 19, 11–28.

914   Brown, T.A., Belt, S.T., Philippe, B., Mundy, C.J., Massé, G., Poulin, M., Gosselin, M.,
915   2011. Temporal and vertical variations of lipid biomarkers during a bottom ice diatom bloom
916   in the Canadian Beaufort Sea: further evidence for the use of the IP_{25} biomarker as a proxy
917   for spring Arctic sea ice. Polar Biology 34, 1857–1868.

918   Brown, T.A., Belt, S.T., Tatarek, A., Mundy, C.J., 2014. Source identification of the Arctic
919   sea ice proxy IP_{25}. Nature Communications 5, 4197.

920   Cabedo-Sanz, P., Belt, S.T., 2016. Seasonal sea ice variability in eastern Fram Strait over the
921   last 2,000 years. Arktos (in press).

922   Cabedo-Sanz, P., Smik, L., Belt, S.T., 2016. On the stability of various highly branched
923   isoprenoid (HBI) lipids in stored sediments and sediment extracts. Organic Geochemistry 97,
924   74–77.
925
926   Calvo, E., Grimalt, J., Jansen, E., 2002. High resolution U^{K}_{37} sea surface temperature
927   reconstruction in the Norwegian Sea during the Holocene. Quaternary Science Reviews 21,
928   1385–1394.

929   Chapman, M.R., Shackleton, N.J., 2000. Evidence of 550-year and 1000-year cyclicities in
930   North Atlantic circulation patterns during the Holocene. The Holocene 10, 287–291.

931   Cronin, T.M., Polyak, L., Reed, D., Kandiano, E.S., Marzen, R.E., Council, E.A., 2013 A
932   600-ka Arctic sea-ice record from Mendeleev Ridge based on ostracodes. Quaternary Science
933   Reviews 79, 157–167.

934　Darling, K.F., Kucera, M., Kroon, D., Wade, C.M., 2006. A resolution for the coiling
935　direction paradox in *Neogloboquadrina pachyderma*. Paleoceanography 21, PA2011.
936　doi:10.1029/2005PA001189.
937
938　de la Mare, W.K., 1997. Abrupt mid-twentieth-century decline in Antarctic sea-ice extent
939　from whaling records. Nature 389, 57-60

940　de Vernal, A., Gersonde, R., Goosse, H., Seidenkrantz, M.-S., Wolff, E.W., 2013a. Sea ice in
941　the paleoclimate system: the challenge of reconstructing sea ice from proxies – an
942　introduction. Quaternary Science Reviews 79, 1–8.

943　de Vernal, A., Hillaire-Marcel, C., Rochon, A., Fréchette, B., Henry, M., Solignac, S.,
944　Bonnet, S., 2013b. Dinocyst-based reconstructions of sea ice cover concentration during the
945　Holocene in the Arctic Ocean, the northern North Atlantic Ocean and its adjacent seas.
946　Quaternary Science Reviews 79, 111–121.

947　de Vernal, A., Rochon, A., Fréchette, B., Henry, M., Radi, T., Solignac, S., 2013c.
948　Reconstructing past sea ice cover of the Northern Hemisphere from dinocyst assemblages:
949　status of the approach. Quaternary Science Reviews 79, 122–134.

950　Dickson, R.R., Meincke, J., Malmberg, S.-A., Lee, A.J., 1988. The "great salinity anomaly"
951　in the northern North Atlantic 1968–1982. Progress in Oceanography 20, 103–151.

952　Divine, D.V., Dick, C., 2006. Historical variability of sea ice edge position in the Nordic
953　Seas. J. Geophys. Res 111, C01001.

954　Dyke, A.S., Hooper, J., Savelle, J.M., 1996. A history of sea ice in the Canadian Arctic
955　Archipelago based on postglacial remains of the bowhead whale (*Balaena mysticetus*). Arctic
956　49, 235–255.

957　Eiríksson, J., Knudsen, K.L., Haflidason, H., Henriksen, P., 2000. Late-glacial and Holocene
958　palaeoceanography of the North Icelandic shelf. Journal of Quaternary Science 15, 23–42.

959　Fahl, K., Stein, R., 2012. Modern seasonal variability and deglacial/Holocene change of
960　central Arctic Ocean sea-ice cover: New insights from biomarker proxy records. Earth and
961　Planetary Science Letters 351, 123–133.

962　Funder, S., Goosse, H., Jepsen, H., Kaas, E., Kjær, K.H., Korsgaard, N.J., Larsen, N.K.,
963　Linderson, H., Lyså, A., Möller, P., 2011. A 10,000-year record of Arctic Ocean sea-ice
964　variability—view from the beach. Science 333, 747–750.

965　Furze, M.F.A., Pienkowski, A.J., Coulthard, R.D., 2014. New cetacean ΔR values for Arctic
966　North America and their implications for marine-mammal-based palaeoenvironmental
967　reconstructions. Quaternary Science Reviews 91, 218–241.

968 Geirsdóttir, Á., Miller, G.H., Axford, Y., Ólafsdóttir, S., 2009. Holocene and latest
969 Pleistocene climate and glacier fluctuations in Iceland. Quaternary Science Reviews 28,
970 2107–2118.

971 Geirsdóttir, Á., Miller, G.H., Larsen, D.J., Ólafsdóttir, S., 2013. Abrupt Holocene climate
972 transitions in the northern North Atlantic region recorded by synchronized lacustrine records
973 in Iceland. Quaternary Science Reviews 70, 48–62.

974 Ghil, M., Allen, M., Dettinger, M., Ide, K., Kondrashov, D., Mann, M., Robertson, A.W.,
975 Saunders, A., Tian, Y., Varadi, F., 2002. Advanced spectral methods for climatic time series.
976 Reviews of Geophysics 40, 3-1-3-41.

977 Giraudeau, J., Jennings, A., Andrews, J., 2004. Timing and mechanisms of surface and
978 intermediate water circulation changes in the Nordic Seas over the last 10,000 calyears: a
979 view from the North Iceland shelf. Quaternary Science Reviews 23, 2127–2139.

980 Goosse, H., Roche, D.M., Mairesse, A., Berger, M., 2013. Modelling past sea ice changes.
981 Quaternary Science Reviews 79, 191–206.

982 Hald, M., Andersson, C., Ebbesen, H., Jansen, E., Klitgaard-Kristensen, D., Risebrobakken,
983 B., Salomonsen, G.R., Sarnthein, M., Sejrup, H.P., Telford, R.J., 2007. Variations in
984 temperature and extent of Atlantic Water in the northern North Atlantic during the Holocene.
985 Quaternary Science Reviews 26, 3423–3440.

986 Haywood, A.M., Valdes, P.J., 2004. Modelling Pliocene warmth: contribution of atmosphere,
987 oceans and cryosphere. Earth and Planetary Science Letters 218, 363–377.

988 Helgadóttir, G., 1997. Paleoclimate (0 to> 14 ka) of W. and NW Iceland: An Iceland/USA
989 Contribution to PALE, Cruise Report B9-97. Marine Research Institute of Iceland.

990 Hopkins, T.S., 1991. The GIN Sea - a synthesis of its physical oceanography and literature
991 review 1972 - 1985. Earth Science Reviews 30, 175–318.

992 Hörner, T., Stein, R., Fahl, K., Birgel, D., 2016. Post-glacial variability of sea ice cover, river
993 run-off and biological production in the western Laptev Sea (Arctic Ocean) – A high-
994 resolution biomarker study. Quaternary Science Reviews 143, 133–149.

995 Jennings, A.E., Weiner, N.J., 1996. Environmental change in eastern Greenland during the
996 last 1300 years: evidence from foraminifera and lithofacies in Nansen Fjord, 68 N. The
997 Holocene 6, 179–191.

998 Jennings, A.E., Knudsen, K.L., Hald, M., Hansen, C.V., Andrews, J.T., 2002. A mid-
999 Holocene shift in Arctic sea-ice variability on the East Greenland Shelf. The Holocene 12,
1000 49–58.

1001   Jennings, A.E., Andrews, J.A., Wilson, L., 2011. Holocene environmental evolution of the
1002   SE Greenland Shelf North and South of the Denmark Strait: Irminger and East Greenland
1003   current interactions. Quaternary Science Reviews 30, 980–998.

1004   Johannessen, T., Jansen, E., Flatøy, A., Ravelo, A.C., 1994. The relationship between surface
1005   water masses, oceanographic fronts and paleoclimatic proxies in surface sediments of the
1006   Greenland, Iceland, Norwegian Seas, Carbon cycling in the glacial ocean: constraints on the
1007   ocean's role in global change. Springer, pp. 61–85.

1008   Jones, P.D., Mann, M.E., 2004. Climate over past millennia. Reviews of Geophysics 42,
1009   RG2002, doi:10.1029/2003RG000143.

1010   Justwan, A., Koç, N., 2008. A diatom based transfer function for reconstructing sea ice
1011   concetrations in the North Atlantic. Marine Micropaleontology 41, 73–96.

1012   Justwan, A., Koç, N., Jennings, A.E., 2008. Evolution of the Irminger and East Icelandic
1013   Current systems through the Holocene, revealed by diatom-based sea surface temperature
1014   reconstructions. Quaternary Science Reviews 27, 1571–1582.

1015   Kaufman, D., Ager, T., Anderson, N., Anderson, P., Andrews, J., Bartlein, P., Brubaker, L.,
1016   Coats, L., Cwynar, L.C., Duvall, M., 2004. Holocene thermal maximum in the western Arctic
1017   (0–180 W). Quaternary Science Reviews 23, 529–560.

1018   Knies, J., Cabedo-Sanz, P., Belt, S.T., Baranwal, S., Fietz, S., Rosell-Melé, A., 2014. The
1019   emergence of modern sea ice cover in the Arctic Ocean. Nature Communications 5, 5608.

1020   Knudsen, K., Jiang, H., Jansen, E., Eiríksson, J., Heinemeier, J., Seidenkrantz, M.-S., 2004.
1021   Environmental changes off North Iceland during the deglaciation and the Holocene:
1022   foraminifera, diatoms and stable isotopes. Marine Micropaleontology 50, 273–305.

1023   Koç, N., Jansen, E., Haflidason, H., 1993. Paleoceanographic reconstructions of surface
1024   ocean conditions in the Greenland, Iceland and Norwegian seas through the last 14 ka based
1025   on diatoms. Quaternary Science Reviews 12, 115–140.

1026   Koch, L., 1945. The East Greenland Ice. Meddelelser om Gronland. 3, 346.

1027   Kristjansdottir, G.B., Moros, M., Andrews, J.T., Jennings, A.E., 2016. Holocene Mg/Ca,
1028   alkenones, and light stable isotope measurements on the outer North Iceland shelf (MD99-
1029   2269): A comparison of proxy data. The Holocene (in press).

1030   Kristjánsdóttir, G.B., Lea, D.W., Jennings, A.E., Pak, D.K., Belanger, C., 2007. New spatial
1031   Mg/Ca ‐ temperature calibrations for three Arctic, benthic foraminifera and reconstruction of
1032   north Iceland shelf temperature for the past 4000 years. Geochemistry, Geophysics,
1033   Geosystems 8, Q03P21, doi:10.1029/2006GC001425.

1034 Larsen, D.J., Miller, G.H., Geirsdóttir, Á., Thordarson, T., 2011. A 3000-year varved record
1035 of glacier activity and climate change from the proglacial lake Hvítárvatn, Iceland.
1036 Quaternary science reviews 30, 2715–2731.

1037 Lehner, F., Born, A., Raible, C.C., Stocker, T.F., 2013. Amplified inception of European
1038 Little Ice Age by sea ice–ocean–atmosphere feedbacks. Journal of Climate 26, 7586–7602.

1039 Malmberg, S.-A., 1985. The water masses between Iceland and Greenland. Journal of Marine
1040 Research 9, 127–140.

1041 Mann, M.E., Lees, J.M., 1996. Robust estimation of background noise and signal detection in
1042 climatic time series. Climatic change 33, 409–445.

1043 Massé, G., Rowland, S.J., Sicre, M.-A., Jacob, J., Jansen, E., Belt, S.T., 2008. Abrupt climate
1044 changes for Iceland during the last millennium: Evidence from high resolution sea ice
1045 reconstructions. Earth and Planetary Science Letters 269, 565–569.

1046 Massé, G., Belt, S.T., Crosta, X., Schmidt, S., Snape, I., Thomas, D.N., Rowland, S.J., 2011.
1047 Highly branched isoprenoids as proxies for variable sea ice conditions in the Southern Ocean.
1048 Antarctic Science 1, 1–12.

1049 McGregor, H.V., Evans, M.N., Goosse, H., Leduc, G., Martrat, B., Addison, J.A., Mortyn,
1050 P.G., Oppo, D.W., Seidenkrantz, M.-S., Sicre, M.-A., 2015. Robust global ocean cooling
1051 trend for the pre-industrial Common Era. Nature Geoscience 8(9), 671–677.

1052 Miller, G.H., Alley, R.B., Brigham-Grette, J., Fitzpatrick, J.J., Polyak, L., Serreze, M.C.,
1053 White, J.W., 2010. Arctic amplification: can the past constrain the future? Quaternary
1054 Science Reviews 29, 1779–1790.

1055 Miller, G.H., Geirsdóttir, Á., Zhong, Y., Larsen, D.J., Otto-Bliesner, B.L., Holland, M.M.,
1056 Bailey, D.A., Refsnider, K.A., Lehman, S.J., Southon, J.R., 2012. Abrupt onset of the Little
1057 Ice Age triggered by volcanism and sustained by sea-ice/ocean feedbacks. Geophysical
1058 Research Letters 39, L02708.

1059 Miller, G.H., Briner, J.P., Refsnider, K.A., Lehman, S.J., Geirsdóttir, Á., Larsen, D.J.,
1060 Southon, J.R., 2013a. Substantial agreement on the timing and magnitude of Late Holocene
1061 ice cap expansion between East Greenland and the Eastern Canadian Arctic: A commentary
1062 on Lowell et al., 2013. Quaternary Science Reviews 77, 239–245.

1063 Miller, G.H., Lehman, S.J., Refsnider, K.A., Southon, J.R., Zhong, Y., 2013b. Unprecedented
1064 recent summer warmth in Arctic Canada. Geophysical Research Letters 40, 5745–5751.

1065 Moossen, H., Bendle, J., Seki, O., Quillmann, U., Kawamura, K., 2015. North Atlantic
1066 Holocene climate evolution recorded by high-resolution terrestrial and marine biomarker
1067 records. Quaternary Science Reviews 129, 111–127.

1068 Moros, M., Andrews, J.T., Eberl, D.D., Jansen, E., 2006. Holocene history of drift ice in the
1069 northern North Atlantic: Evidence for different spatial and temporal modes.
1070 Paleoceanography 21, PA2017.

1071 Moros, M., Jansen, E., Oppo, D.W., Giraudeau, J., Kuijpers, A., 2012. Reconstruction of the
1072 late-Holocene changes in the Sub-Arctic Front position at the Reykjanes Ridge, north
1073 Atlantic. The Holocene 22, 877–886.

1074 Müller, J., Massé, G., Stein, R., Belt, S.T., 2009. Variability of sea-ice conditions in the Fram
1075 Strait over the past 30,000 years. Nature Geoscience 2, 772–776.

1076 Müller, J., Wagner, A., Fahl, K., Stein, R., Prange, M., Lohmann, G., 2011. Towards
1077 quantitative sea ice reconstructions in the northern North Atlantic: A combined biomarker
1078 and numerical modelling approach. Earth and Planetary Science Letters 306, 137–148.

1079 Müller, J., Werner, K., Stein, R., Fahl, K., Moros, M., Jansen, E., 2012. Holocene cooling
1080 culminates in sea ice oscillations in Fram Strait. Quaternary Science Reviews 47, 1–14.

1081 Müller, J., Stein, R., 2014. High-resolution record of late glacial sea ice changes in Fram
1082 Strait corroborates ice-ocean interactions during abrupt climate shifts. Earth and Planetary
1083 Science Letters 403, 446–455.

1084 Navarro-Rodriguez, A., Belt, S.T., Brown, T.A., Knies, J., 2013. Mapping recent sea ice
1085 conditions in the Barents Sea using the proxy biomarker IP_{25}: implications for palaeo sea ice
1086 reconstructions. Quaternary Science Reviews 79, 26–39.

1087 Ogilvie, A.E., 1996. Sea-ice conditions off the coasts of Iceland AD 1601–1850 with special
1088 reference to part of the Maunder Minimum period (1675–1715). Arkeoologisk Museum i
1089 Stavanger 25, 9–12.

1090 Ogilvie, A.E., Barlow, L.K., Jennings, A., 2000. North Atlantic climate c. AD 1000:
1091 Millennial reflections on the Viking discoveries of Iceland, Greenland and North America.
1092 Weather 55, 34–45.

1093 Ogilvie, A.E., Jónsdóttir, I., 2000. Sea ice, climate, and Icelandic fisheries in the eighteenth
1094 and nineteenth centuries. Arctic 53, 383–394.

1095 Ogilvie, A.E., Jónsson, T., 2001. "Little Ice Age" research: a perspective from Iceland.
1096 Climatic Change 48, 9–52.

1097 Ólafsdóttir, K.B., Geirsdóttir, Á., Miller, G.H., Larsen, D.J., 2013. Evolution of NAO and
1098 AMO strength and cyclicity derived from a 3-ka varve-thickness record from Iceland.
1099 Quaternary Science Reviews 69, 142–154.

1100   Ólafsdóttir, S., Jennings, A.E., Geirsdóttir, Á., Andrews, J., Miller, G.H., 2010. Holocene
1101   variability of the North Atlantic Irminger current on the south- and northwest shelf of
1102   Iceland. Marine Micropaleontology 77, 101–118.

1103   Ólafsson, J., 1999. Connections between oceanic conditions off N-Iceland, Lake Myvatn
1104   temperature, regional wind direction variability and the North Atlantic Oscillation. Rit
1105   Fiskideild 16, 41–58.

1106   Paillard, D., Labeyrie, L., Yiou, P., 1996. Macintosh program performs time‐series analysis.
1107   Eos, Transactions American Geophysical Union 77, 379.

1108   Perner, K., Moros, M., Lloyd, J.M., Jansen, E., Stein, R., 2015. Mid to late Holocene
1109   strengthening of the East Greenland Current linked to warm subsurface Atlantic water.
1110   Quaternary Science Reviews 129, 296–307.

1111   Polyak, L., Belt, S.T., Cabedo-Sanz, P., Yamamoto, M., Park, Y.-H., 2016. Holocene sea-ice
1112   conditions and circulation at the Chukchi-Alaskan margin, Arctic Ocean, inferred from
1113   biomarker proxies. The Holocene (in press).

1114   Polyak, L., Alley, R.B., Andrews, J.T., Brigham-Grette, J., Cronin, T.M., Darby, D.A., Dyke,
1115   A.S., Fitzpatrick, J.J., Funder, S., Holland, M., Jennings, A.E., Miller, G.H., O´Regan, M.,
1116   Savelle, J., Serreze, M., John, K.S., White, J.W.C., Wolff, E., 2010. History of sea ice in the
1117   Arctic. Quaternary Science Reviews 29, 1757–1778.

1118   Ram, M., Stolz, M.R., 1999. Possible solar influences on the dust profile of the GISP2 ice
1119   core from central Greenland. Geophysical Research Letters 26, 1043–1046.

1120   Rasmussen, T.L., Forwick, M., Mackensen, A., 2012. Reconstruction of inflow of Atlantic
1121   Water to Isfjorden, Svalbard during the Holocene: Correlation to climate and seasonality.
1122   Marine Micropaleontology 94–95, 80–90.

1123   Renssen, H., Goosse, H., Fichefet, T., 2005. Contrasting trends in North Atlantic deep‐
1124   water formation in the Labrador Sea and Nordic seas during the Holocene. Geophysical
1125   Research Letters 32, L08711, doi:10.1029/2005GL022462

1126   Risebrobakken, B., Jansen, E., Andersson, C., Mjelde, E., Hevrøy, K., 2003. A high‐
1127   resolution study of Holocene paleoclimatic and paleoceanographic changes in the Nordic
1128   Seas. Paleoceanography 18, 1017, doi:10.1029/2002PA000764.

1129   Risebrobakken, B., Dokken, T., Smedsrud, L., Andersson, C., Jansen, E., Moros, M.,
1130   Ivanova, E., 2009. Early Holocene temperature variability in the Nordic Seas: The role of
1131   oceanic heat advection versus changes in orbital forcing. Paleoceanography 26, PA4206.

1132   Rodionov, S.N., 2004. A sequential algorithm for testing climate regime shifts. Geophysical
1133   Research Letters 31, L09204.

1134 Rodionov, S.N., 2006. Use of prewhitening in climate regime shift detection. Geophysical
1135 Research Letters 33, L12707.

1136 Rowland, S., Allard, W., Belt, S., Massé, G., Robert, J.-M., Blackburn, S., Frampton, D.,
1137 Revill, A., Volkman, J., 2001. Factors influencing the distributions of polyunsaturated
1138 terpenoids in the diatom, Rhizosolenia setigera. Phytochemistry 58, 717–728.

1139 Rudels, B., Fahrbach, E., Meincke, J., Budéus, G., Eriksson, P., 2002. The East Greenland
1140 Current and its contribution to the Denmark Strait overflow. ICES Journal of Marine Science:
1141 Journal du Conseil 59, 1133–1154.

1142 Sarnthein, M., Kreveld, S., Erlenkeuser, H., Grootes, P., Kucera, M., Pflaumann, U., Schulz,
1143 M., 2003a. Centennial-to-millennial-scale periodicities of Holocene climate and sediment
1144 injections off the western Barents shelf, 75˚N. Boreas 32, 447–461.

1145 Sarnthein, M., Pflaumann, U., Weinelt, M., 2003b. Past extent of sea ice in the northern
1146 North Atlantic inferred from foraminiferal paleotemperature estimates. Paleoceanography 18,
1147 1047.

1148 Schiermeier, Q., 2012. Ice loss shifts Arctic cycles. Nature 489, 185–186.

1149 Schleussner, C., Feulner, G., 2013. A volcanically triggered regime shift in the subpolar
1150 North Atlantic Ocean as a possible origin of the Little Ice Age. Climate of the Past 9, 1321–
1151 1330.

1152 Seidenkrantz, M.S., 2013. Benthic foraminifera as palaeo sea-ice indicators in the subarctic
1153 realm – examples from the Labrador Sea–Baffin Bay region. Quaternary Science Reviews 79,
1154 135–144.

1155 Serreze, M.C., Barrett, A.P., Slater, A.G., Steele, M., Zhang, J., Trenberth, K.E., 2007. The
1156 large-scale energy budget of the Arctic. Journal of Geophysical Research 112, D11122.

1157 Sicre, M.A., Yiou, P., Eiríksson, J., Ezat, U., Guimbaut, E., Dahhaoui, I., Knudsen, K.-L.,
1158 Jansen, E., Turon, J.-L., 2008. A 4500-year reconstruction of sea surface temperature
1159 variability at decadal time-scales off North Iceland. Quaternary Science Reviews 27, 2041–
1160 2047.

1161 Sicre, M.A., Hall, I.R., Mignot, J., Khodri, M., Ezat, U., Truong, M.X., Eiríksson, J.,
1162 Knudsen, K.L., 2011. Sea surface temperature variability in the subpolar Atlantic over the
1163 last two millennia. Paleoceanography 26, PA4218.

1164 Sicre, M.A., Khodri, M., Mignot, J., Eiríksson, J., Knudsen, K.L., Ezat, U., Closset, I.,
1165 Nogues, P., Massé, G., 2013. Sea surface temperature and sea ice variability in the subpolar
1166 North Atlantic from explosive volcanism of the late thirteenth century. Geophysical Research
1167 Letters 40, 5526–5530.

1168 Sicre, M.A., Weckström, K., Seidenkrantz, M.-S., Kuijpers, A., Benetti, M., Massé, G., Ezat,
1169 U., Schmidt, S., Bouloubassi, I., Olsen, J., 2014. Labrador current variability over the last
1170 2000 years. Earth and Planetary Science Letters 400, 26–32.

1171 Smik, L., Belt, S.T., Lieser, J.L., Armand, L.K., Leventer, A., 2015. Distributions of highly
1172 branched isoprenoid alkenes in surface waters from East Antarctica: Further insights for
1173 biomarker-based paleo sea-ice reconstruction. Organic Geochemistry 95, 71–80.

1174 Smik, L., Cabedo-Sanz, P., Belt, S.T., 2016. Semi-quantitative estimates of paleo Arctic sea
1175 ice concentration based on source-specific highly branched isoprenoid alkenes: a further
1176 development of the PIP_{25} index. Organic Geochemistry 92, 63–69.

1177 Solignac, S., Giraudeau, J., de Vernal, A., 2006. Holocene sea surface conditions in the
1178 western North Atlantic: Spatial and temporal heterogeneities. Paleoceanography 21, PA2004.

1179 Stoner, J.S., Jennings, A., Kristjánsdóttir, G.B., Dunhill, G., Andrews, J.T., Hardardóttir, J.,
1180 2007. A paleomagnetic approach toward refining Holocene radiocarbon-based chronologies:
1181 Paleoceanographic records from the north Iceland (MD99-2269) and east Greenland (MD99-
1182 2322) margins. Paleoceanography 22, PA1209.

1183 Stuiver, M., Grootes, P.M., Braziunas, T.F., 1995. The GISP2 δ18O climate record of the
1184 past 16,500 years and the role of the sun, ocean, and volcanoes. Quaternary Research 44,
1185 341–354.

1186 Telesiński, M.M., Spielhagen, R.F., Lind, E.M., 2014. A high‐resolution Lateglacial and
1187 Holocene palaeoceanographic record from the Greenland Sea. Boreas 43, 273–285.

1188 Thomson, D., 1990. Time series analysis of Holocene climate data. Philosophical
1189 Transactions of the Royal Society of London A: Mathematical, Physical and Engineering
1190 Sciences 330, 601–616.

1191 Vare, L.L., Massé, G., Gregory, T.R., Smart, C.W., Belt, S.T., 2009. Sea ice variations in the
1192 central Canadian Arctic Archipelago during the Holocene. Quaternary Science Reviews 28,
1193 1354–1366.

1194 Vare, L.L., Massé, G., Belt, S.T., 2010. A biomarker-based reconstruction of sea ice
1195 conditions for the Barents Sea in recent centuries. The Holocene 20, 637–643.

1196 Wallevik, J.E., Sigurjonsson, H., 1998. The Koch Index. Formulation, Correction and
1197 Extension. Icelandic Meteorological Office Report.

1198 Walker, M.J.C., Berkelhammer, M., Bjorck, S., Cwynar, L.C., Fisher, D.A., Long, A.J.,
1199 Lowe, J.J., Newnham, R.M., Rasmussen, S.O., Weiss, H., 2012. Formal subdivision of the
1200 Holocene Series/Epoch: a Discussion Paper by a Working Group of INTIMATE (Integration
1201 of ice-core, marine and terrestrial records) and the Subcommission on Quaternary
1202 Stratigraphy (International Commission on Stratigraphy). Journal of Quaternary Science 27,
1203 649–659.

1204   Werner, K., Spielhagen, R.F., Bauch, D., Hass, H.C., Kandiano, E., 2013. Atlantic Water
1205   advection versus sea‐ice advances in the eastern Fram Strait during the last 9 ka:
1206   Multiproxy evidence for a two-phase Holocene. Paleoceanography 28, 283–295.

1207   Xiao, X., Stein, R., Fahl,K., 2015. MIS 3 to MIS 1 temporal and LGM spatial variability in
1208   Arctic Ocean sea ice cover: Reconstruction from biomarkers. Paleoceanography, 30,
1209   PA002814.

1210   Zhong, Y., Miller, G., Otto-Bliesner, B., Holland, M., Bailey, D., Schneider, D., Geirsdottir,
1211   A., 2011. Centennial-scale climate change from decadally-paced explosive volcanism: a
1212   coupled sea ice-ocean mechanism. Climate Dynamics 37, 2373–2387.

9 – Figure Legends

Figure 1: (a) Location map showing the B997 surface sediments (black dots) and cores under study (purple diamonds): MD99-2269 and JR51-GC35. Other cores mentioned in this paper (green squares) are: MD99-2263 (2263, Andrews et al., 2009a), MD99-2275 (2275, Massé et al., 2008) and MD99-2273 (2273, Sicre et al., 2013). Main surface water currents are the cold East Greenland Current (EGC) carried southwards along the east coast of Greenland, and the relatively warm Irminger Current (IC), a branch of the North Atlantic Current that flows northward carrying Atlantic waters. The cold East Iceland Current (EIC) and the warm North Iceland Irminger Current (NIIC), together with Denmark Strait (DS) are also indicated; (b) Map showing mean annual sea surface temperatures (0–10 m; bar units are in degrees Celsius) from 1955–2012 obtained from the World Ocean Atlas database. Dotted vertical lines show the location of two routinely surveyed sections, Hornbanki and Siglunes.

Figure 2: Surface sediments from W/N Iceland shelves scaled (red dots) to the abundance of (a) IP_{25};(b) quartz and (c) $C_{25:3}$. Black dots represent locations where proxies were absent (below limit of detection). Blue and black dashed lines indicate the average April location of the sea ice margin AD 1870–1920 and AD 1989–2002, respectively (http://nsidc.org/data.gis/data.html).

Figure 3: Temporal concentration profiles of the sea ice proxies IP_{25} and quartz (Andrews et al., 2014) in (a) MD99-2269 and (b) JR51-GC35. Regime shifts in the IP_{25} data for MD99-2269 are indicated with a black line. Linear regression analyses between IP_{25} and quartz gave correlation coefficients (R^2) of 0.74 and 0.66 for MD99-2269 (25 yr equi-spaced time series) and JR51-GC35 (100 yr equi-spaced time series), respectively. The alkenone-based SST

estimates for MD99-2269 (Kristjansdottir et al., in press) and JR51-GC35 (Bendle and Rosell-Melé, 2007) are also shown.

Figure 4: Temporal percentage profiles and trends of (a) *T. quinqueloba* and (b) *N. pachyderma* in MD99-2269.

Figure 5: Temporal concentration profiles of IP_{25} in (a) JR51-GC35; (b) MD99-2269; (c) MD99-2263 (Andrews et al., 2009a) and (d) MD99-2275 (Massé et al., 2008). (e) Historical Koch sea ice index (Wallevik and Sigurjonsson, 1998).

Figure 6: PCA of the various proxies used in the current study. IP_{25}, $C_{25:3}$, *T. quinqueloba* and *N. pachyderma* data are from the current investigation; Quartz (Moros et al., 2006), $CaCO_3$ (Giraudeau et al., 2004) and SST (Bendle and Rosell-Melé, 2007; Kristjansdottir et al., in press) data are from previously published studies.

Figure 7: Compilation of summer insolation and proxy data for MD99-2269. (a) Summer insolation at 65 °N (Berger and Loutre, 1991); Temporal palaeoclimate profiles and trends for the MD99-2269 core: (b) Biogenic $CaCO_3$ (%) (Giraudeau et al., 2004); (c) $C_{25:3}$ concentrations; (d) *T. quinqueloba* (%); (e) estimated SST (°C) derived from diatoms (Justwan et al., 2008) and alkenones (Kristjansdottir et al., in press); (f) *N. pachyderma* (%); (g) Quartz (%) (Moros et al., 2006); (h) IP_{25} concentrations. The vertical dotted lines at ca 6.2 cal ka BP and ca 3.3 cal ka BP indicate the division between the early-mid Holocene and mid-late Holocene transitions, respectively. The vertical dotted line at ca 1.5 cal ka BP shows the sub-division during the late Holocene.

Figure 8: Compilation of sea ice proxy records for various regions together with a combined terrestrial record for Iceland. (a) Summer insolation at 65 °N (Berger and Loutre, 1991); (b) IP_{25} concentrations in MSM5/5-723-2 (Müller et al., 2012); (c) IP_{25} concentrations in PS2641-4 (Müller et al., 2012); (d) Quartz (%) in MD99-2269 (Moros et al., 2006); (e) IP_{25} concentrations in MD99-2269 and regime shifts trend (black line); (f) Composite multiproxy Hvitarvatn/Haukadalsvatn summer reconstruction from Icelandic lakes (Geirsdóttir et al., 2013). Vertical blue lines represent periods of abrupt change as recorded by the lake composite record. Horizontal dotted lines indicate mean values for quartz, IP_{25} and normalized values for the lake composite record.

Fig. 9: MTM spectra (Mann and Lees, 1996) of the drift ice proxies (resolved at 30 years per sample using Analyseries) in core MD99-2269 over the last ca 8 ka BP: (a) IP_{25}; (b) quartz. Prior to performing the spectral analysis, both time series were detrended by subtracting the first SSA component from the time series.

Supplementary Table 1. Summary of station numbers, locations, water depths, biomarker concentrations and quartz percentage for the surface sediments described in the current study.

Supplementary Table 2: Summary of chronology and biomarker data for MD99-2269

Supplementary Table 3: Summary of chronology and foraminifera data for MD99-2269.

Supplementary Table 4: Summary of chronology and IP_{25} data for JR51-GC35.

Supplementary Figure 1. ^{14}C-based age models for MD99-2269 (Stoner et al., 2007) and JR51-GC35 (Bendle and Rosell-Melé, 2007).
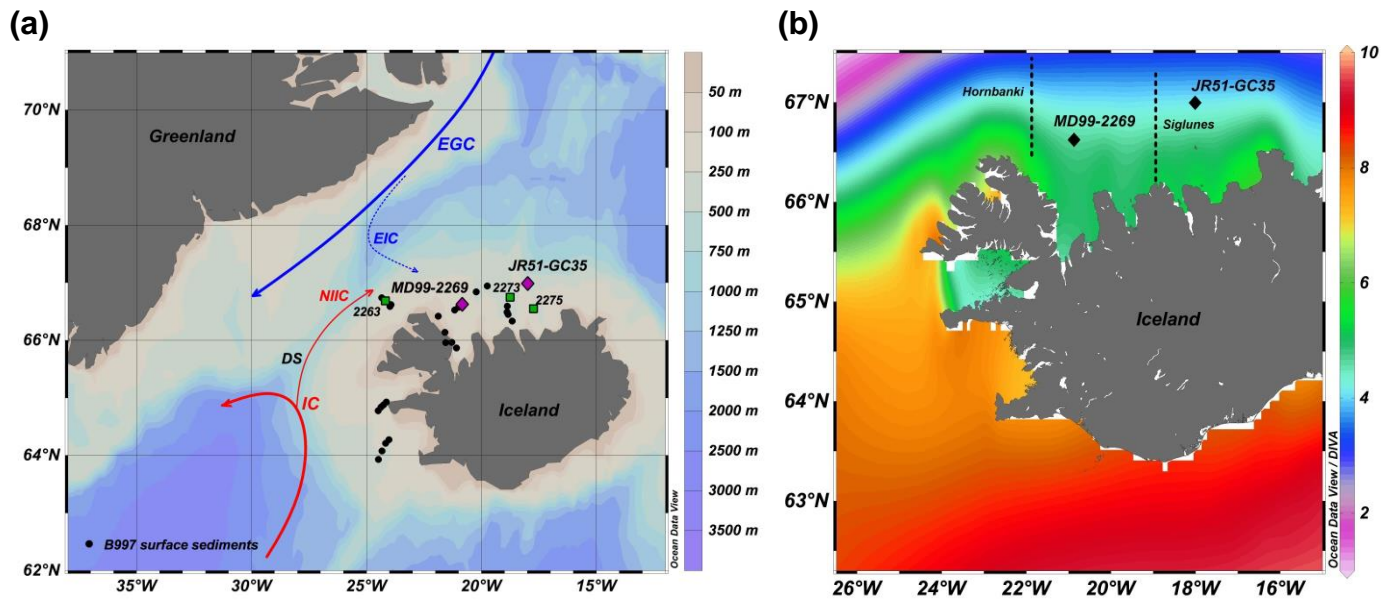
Figure 1_revised

(a)

(b)

Figure 2_revised

(a) IP$_{25}$

(b) Quartz

(c) C$_{25:3}$
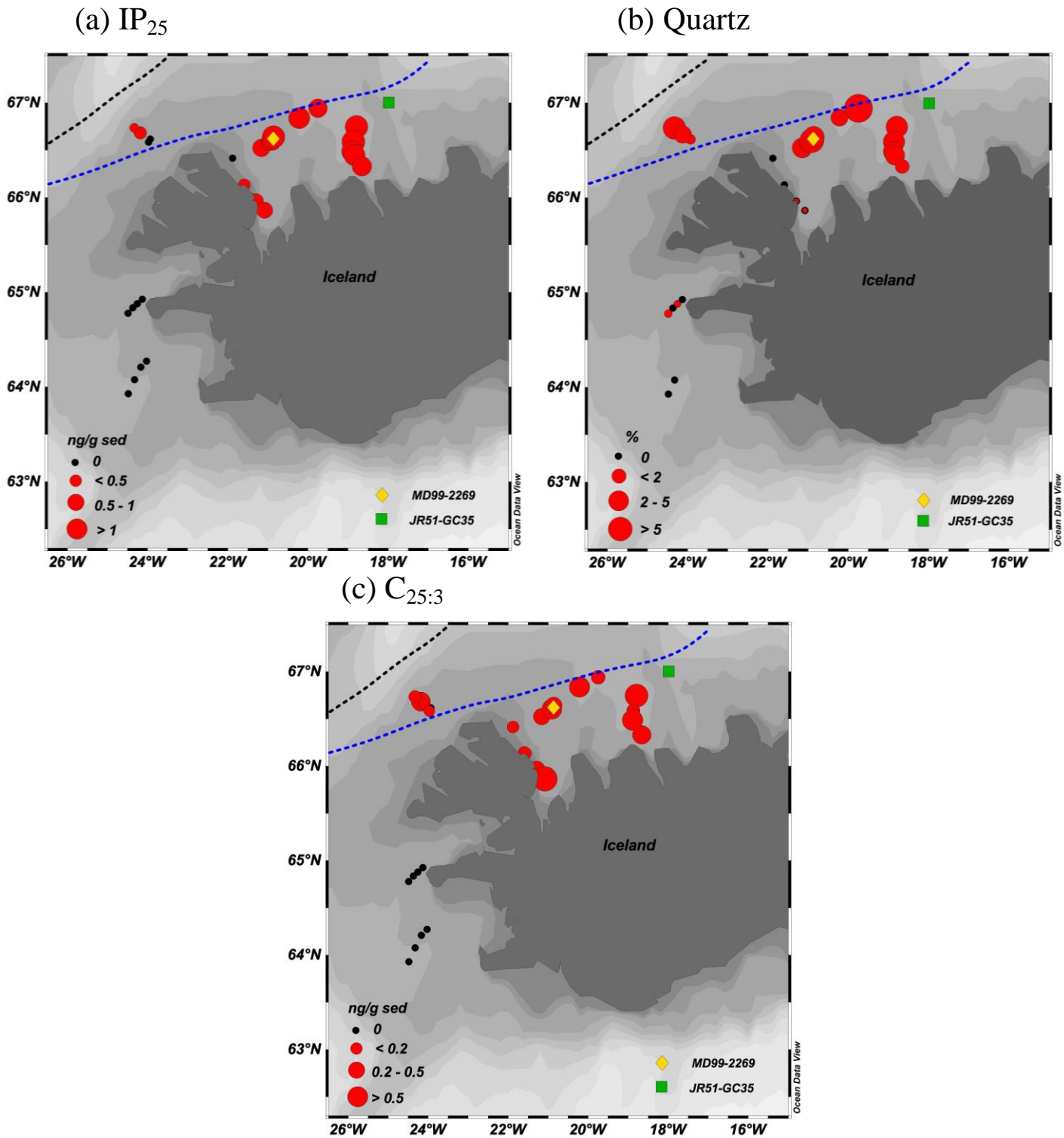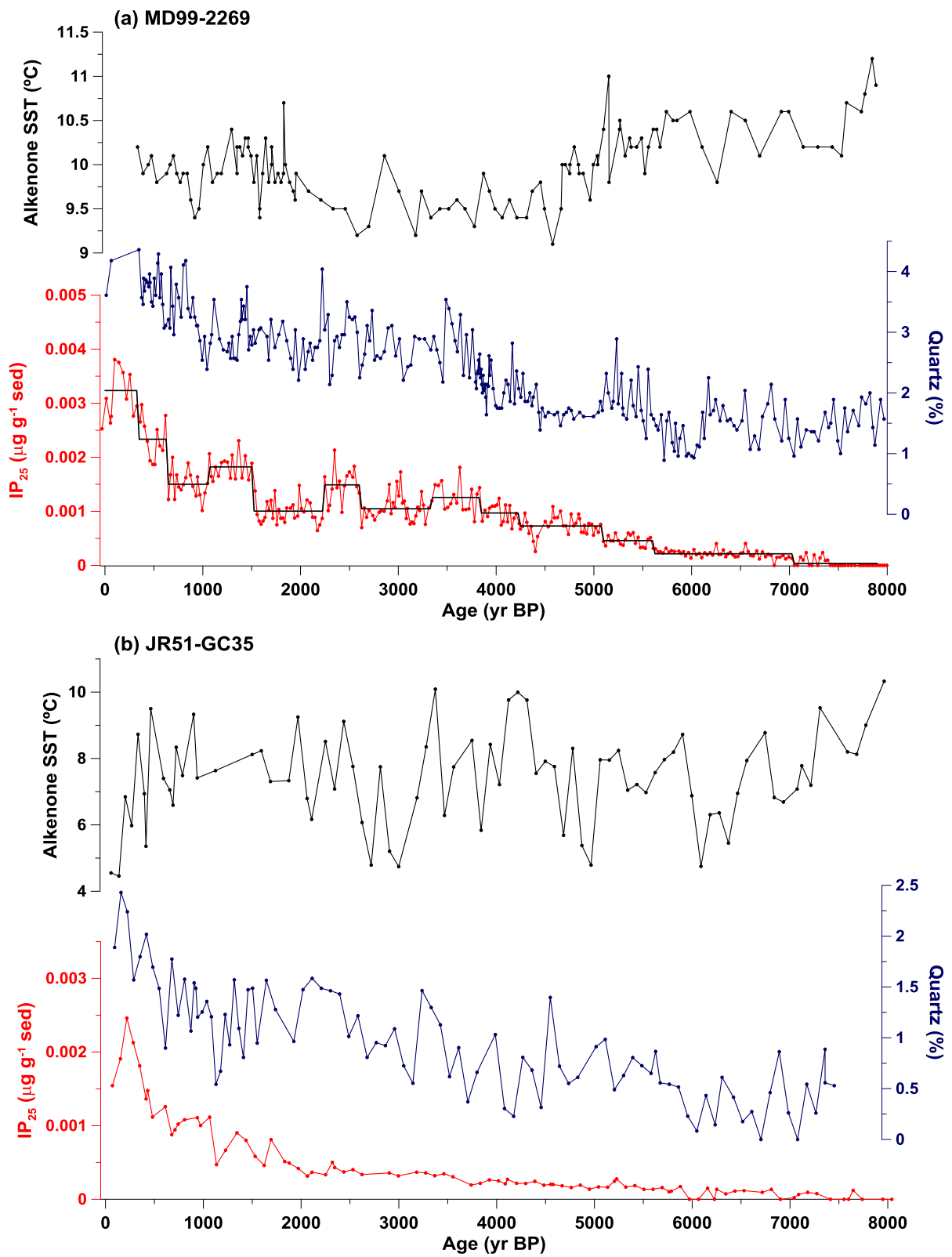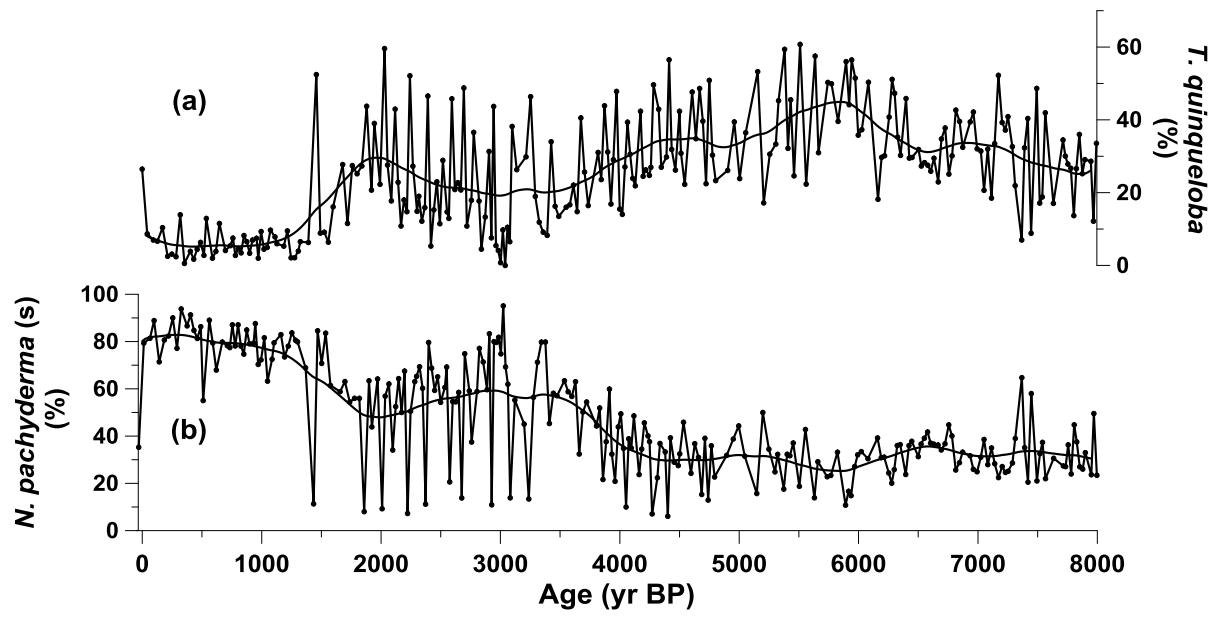
Figure 3_revised

Figure 4_revised

Figure 5_revised

Figure 6_revised

Figure 7_revised
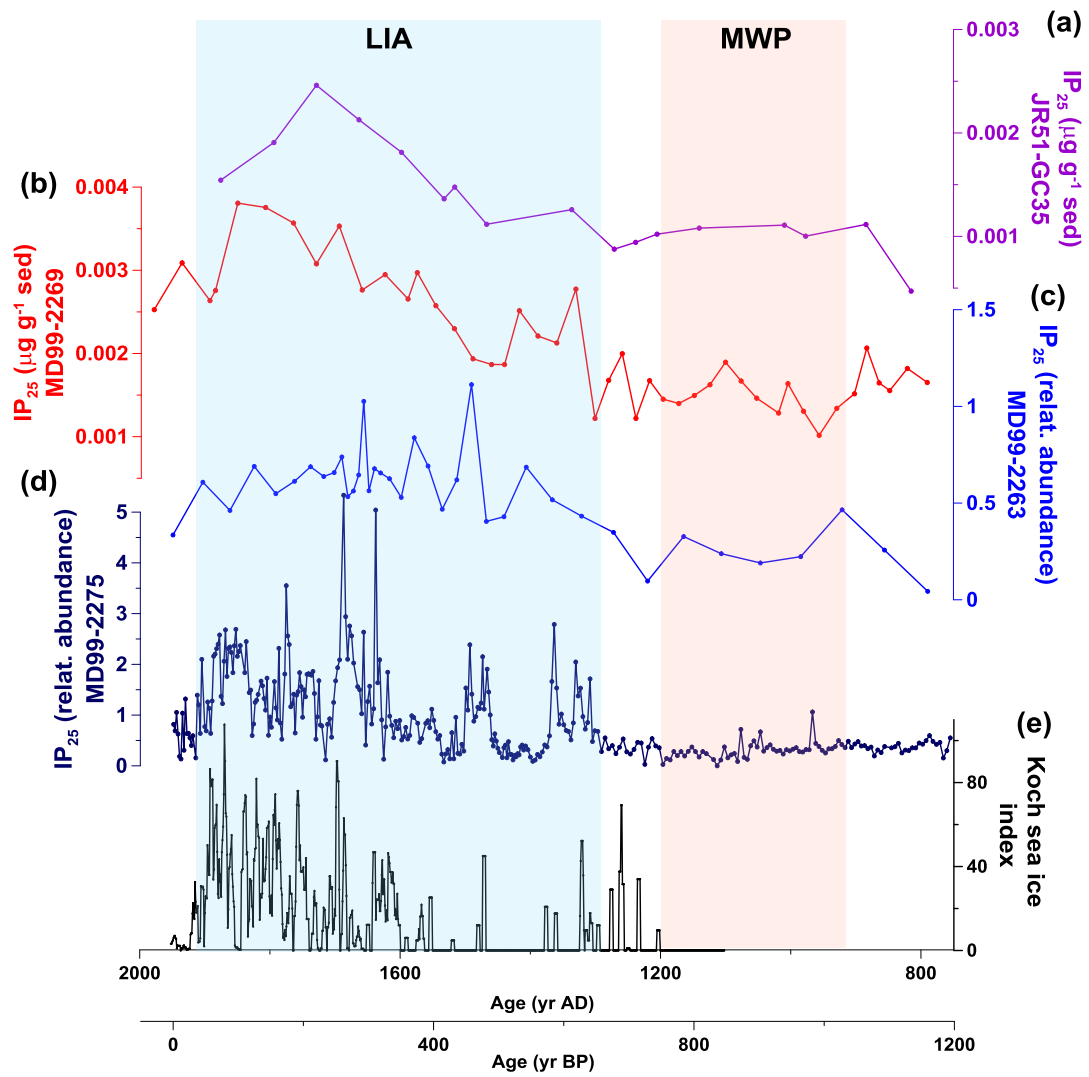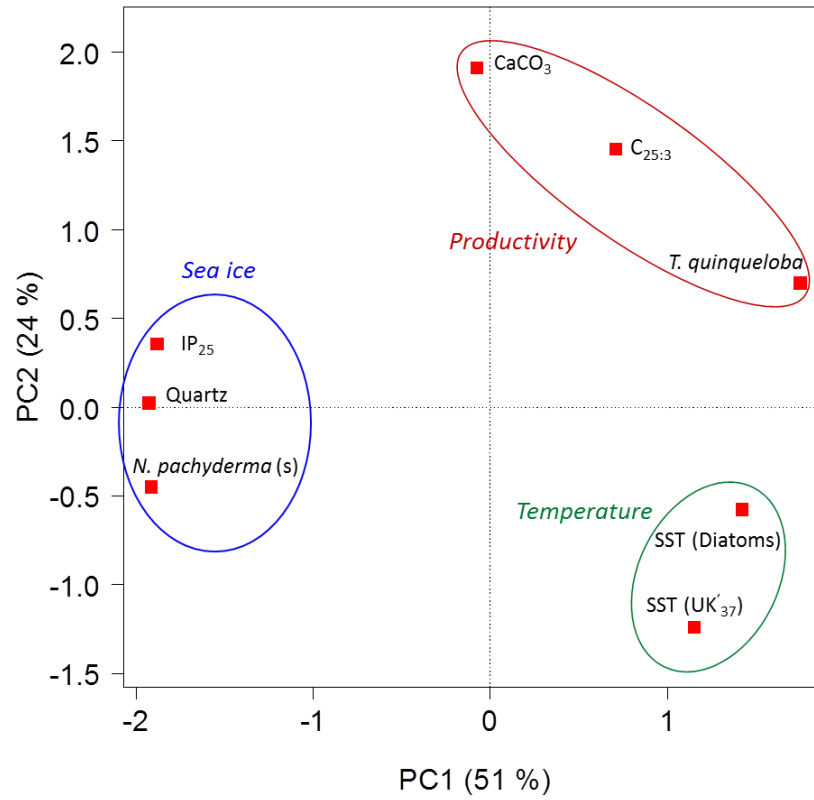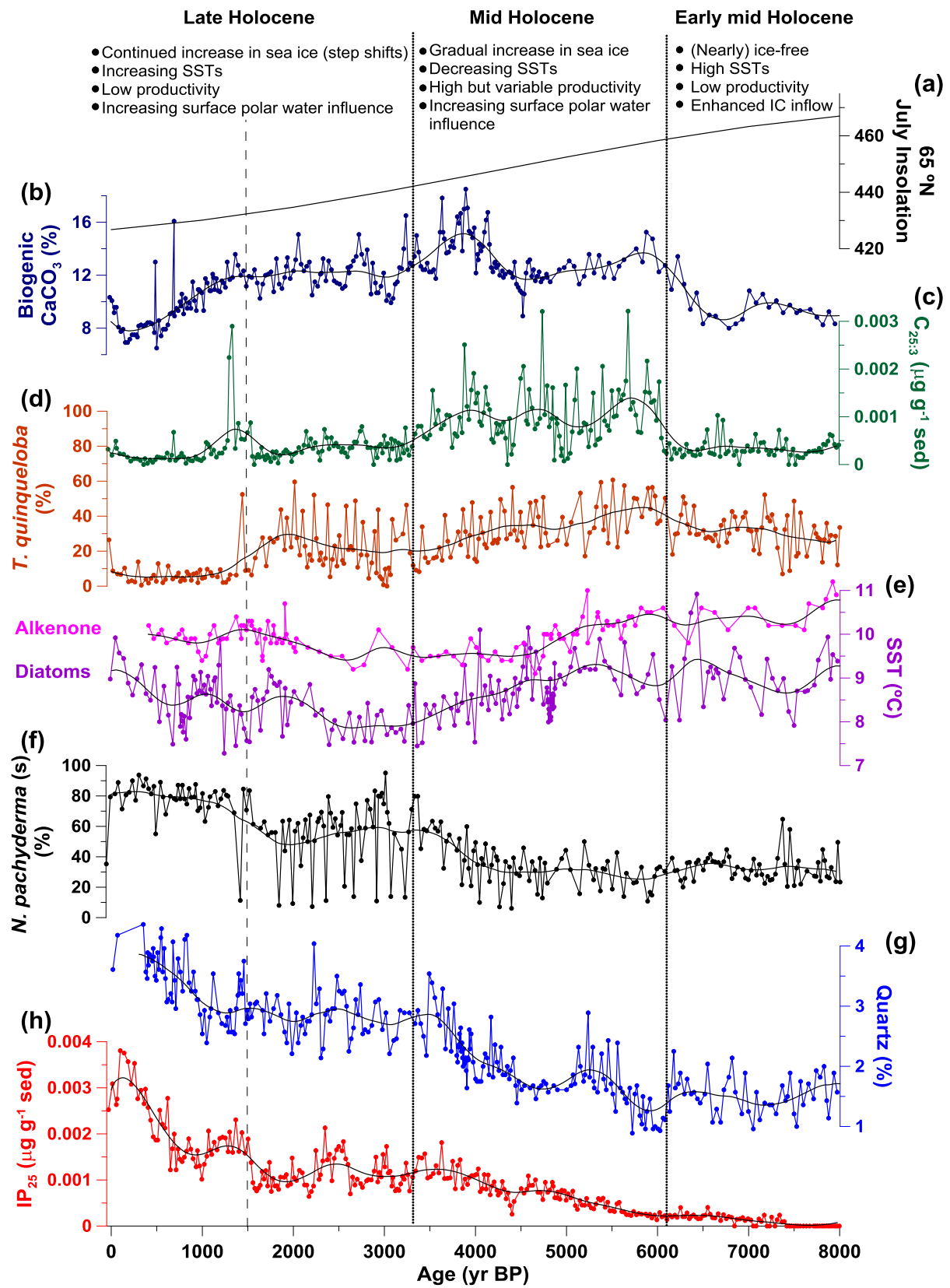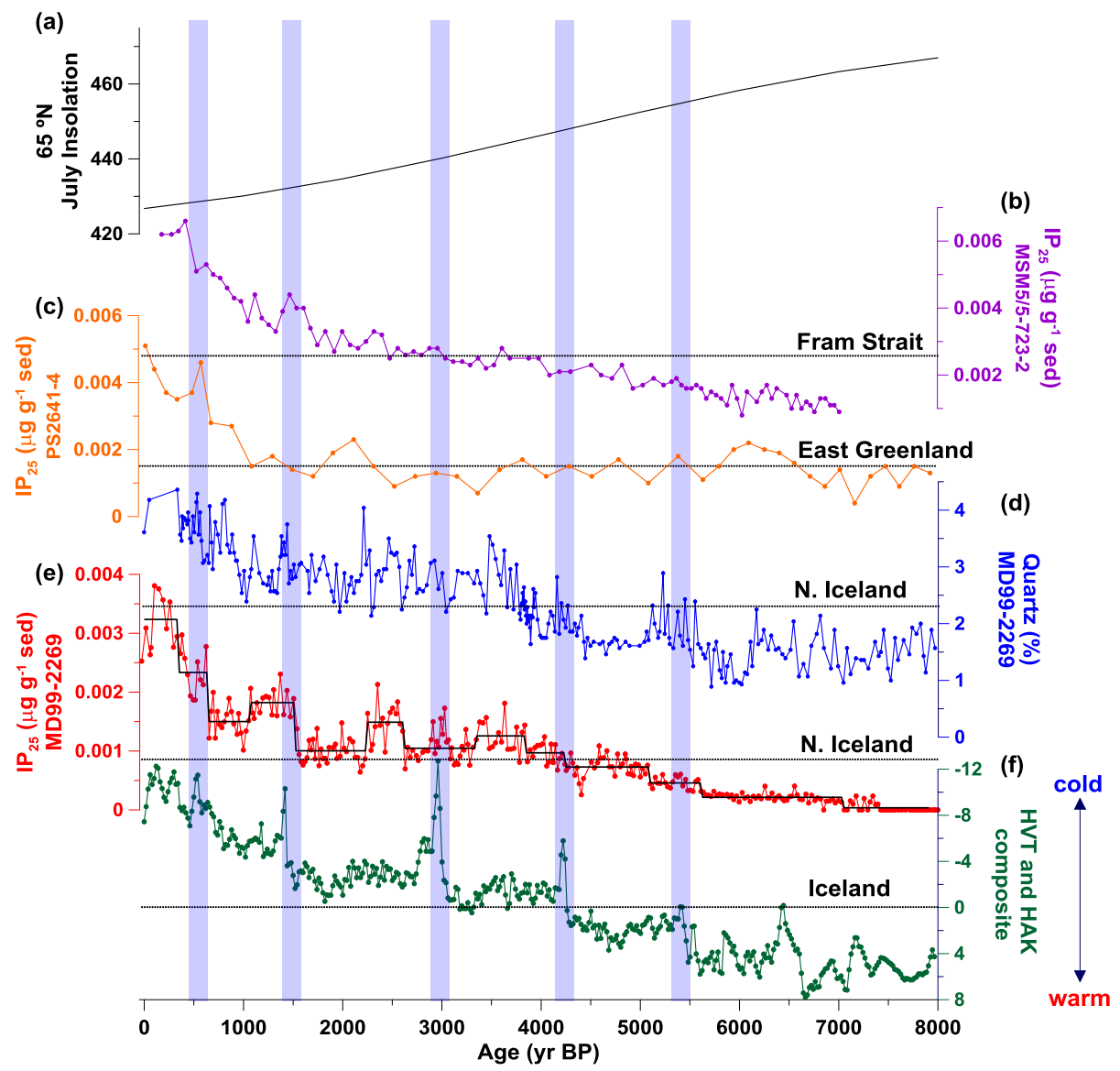

Late Holocene	Mid Holocene	Early mid Holocene
• Continued increase in sea ice (step shifts) • Increasing SSTs • Low productivity • Increasing surface polar water influence	• Gradual increase in sea ice • Decreasing SSTs • High but variable productivity • Increasing surface polar water influence	• (Nearly) ice-free • High SSTs • Low productivity • Enhanced IC inflow

58

Figure 8_revised

Figure 9_revised

(a) IP$_{25}$

(b) Quartz